

THE EFFECTS OF INCREASING EUROPIUM AND
SODIUM CONCENTRATION ON THE IONIC
CONDUCTIVITY IN ALUMINOSILICATE
GLASSES

By

ROBERT ASCIO

Bachelor of Science

Oklahoma State University

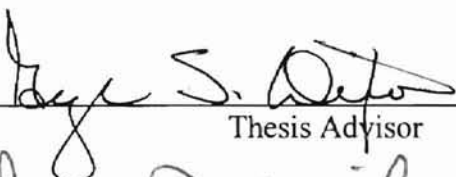
Stillwater, OK

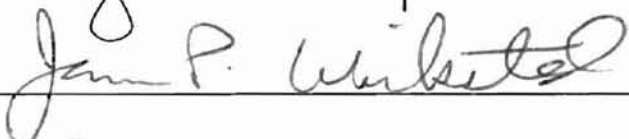
1998

Submitted to the Faculty of the
Graduate College of the
Oklahoma State University
In partial fulfillment of
The requirements for
The Degree of
MASTER OF SCIENCE
May, 2001

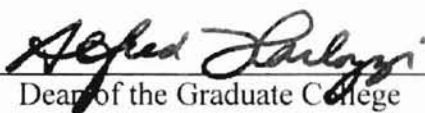
THE EFFECTS OF INCREASING EUROPIUM AND
SODIUM CONCENTRATION ON THE IONIC
CONDUCTIVITY IN ALUMINOSILICATE
GLASSES

Thesis Approved:


Thesis Advisor






Dean of the Graduate College

ACKNOWLEDGEMENTS

I would like to express my gratitude to the entire physics faculty responsible for helping me in my education at Oklahoma State University, especially my adviser, Dr. George S. Dixon. I thank you for giving me the opportunity to do research. I also thank you for your advice, support, and unending patience as my professor. I would also like to thank the members of my thesis committee, Dr. James Wicksted, and Dr. Joel Martin for taking the time to read this thesis. I am also grateful to Dr. Abdul Hamad and Mike Hogsed for introducing me to the techniques of glass sample preparation. I would also like to thank Brandy White, the original “spaghetti” programmer of the lock-in amplifier.

My thanks and love goes to my pets, and good friends. Of my pets, Friendly, Daphne, and Quad, I thank you for the countless torments of begging for food, but all three of you remind me that life is precious. Of my friends, Brandy White, thank you for being my best friend, and also for doing all of my homework. Michael Moon, thank you for encouraging me to go on during my time as an undergraduate and graduate student. John Kernal, thank you for letting me “torment” you for fun.

My special thanks goes to my teacher Mrs. Canon of Raymondville High School, Texas. Thank you for your tireless efforts to help me learn the English language after school hours.

TABLE OF CONTENTS

	Page
I. INTRODUCTION.....	1
1.1 Structure of Silicate Glass.....	2
1.2 Ionic Conductivity of Silicate Glass.....	12
1.3 Impedance Spectroscopy.....	19
II. EXPERIMENTAL METHODS.....	27
2.1 Measuring Techniques.....	27
2.2 Experimental Setup.....	33
2.3 Sample Preparation.....	36
2.4 Experimental Procedure.....	37
III. RESULTS AND DISCUSSION.....	42
3.1 Activation Energy and Conductivity.....	42
3.2 Dielectric Analysis.....	53
3.3 Conclusions on Laser Induced Grating Experiments.....	61
IV. CONCLUSION.....	65
REFERENCES.....	67

LIST OF TABLES

Table	Page
2.0 Sample compositions.....	38
2.1 Sample dimensions.....	39
3.1 Activation energy of Eu and Na samples.....	45
3.2 Exponential pre-factor of Eu and Na Samples.....	49

LIST OF FIGURES

Figure	Page
1.0.a Radial Distribution Function.....	4
1.0.b Diagram of Neighboring SiO ₄	4
1.1 Schematic of SiO ₂ glass network.....	7
1.2 Schematic of ModifiedSiO ₂ Network.....	8
1.3 Aluminosilica glass with europium dopants.....	10
1.4 Periodic Potential Wells (after ref. 6).....	13
1.5 Hypothetical Potential Wells (after ref. 6).....	18
1.6a RC pair circuit.....	21
1.6b Impedance plot of RC pair.....	21
1.7a RC pair in series with capacitor.....	21
1.7b Impedance plot of RC pair in series with capacitor.....	21
2.0 Basic Wheatstone bridge.....	28
2.1 SRS 830 DSP Lock-in Amplifier.....	32
2.2 Experimental Setup.....	34
2.3 Sample Holder.....	35
2.4 Nyquist Plot of 6% Eu.....	39
3.1 σT vs. 1000/T of Europium Series.....	43
3.2 Conductivity vs. Europium Concentration.....	47
3.3 Activation Energy vs. Europium Concentration.....	48
3.4 σT vs. 1000/t of Sodium Series.....	50
3.5 Conductivity vs. Sodium Concentration.....	51

Figure	Page
3.6 Activation Energy vs. Sodium Concentration.....	52
3.7.a M' vs. Frequency of 25% Na.....	54
3.7.b M' vs. Frequency of 12% Eu.....	55
3.7.c M''/M''_{peak} vs. Frequency at 104 C (Eu).....	57
3.7.d M''/M''_{peak} vs. Frequency at 104 C (Na).....	58
3.8.a Dielectric constant vs. Frequency at 102C (Eu).....	59
3.8.b Dielectric constant vs. Frequency at 102C (Na).....	60
3.9.a Loss Angle vs. Frequency for Europium Series at 104C.....	62
3.9.b Loss Angle vs. Frequency for Sodium Series at 104C.....	63

CHAPTER I

INTRODUCTION

A well-known insulator, optical glass exhibits electrical conduction as a function of increasing temperature. For many decades, the temperature dependent conductivity of glass has been studied experimentally. Thermally activated ionic transport over random energy barriers is believed to be the primary contributor in glass conductivity.

Recent developments have found use of glass in digital telecommunications, i.e. fiber-optics higher data transfer bandwidth compared to the traditional copper wire is much more useful in high-speed telecommunications. In the past two decades, laser-induced gratings (LIG) in various glasses are being developed in four-wave mixing experiments. Even though LIG is well established in crystalline materials, there are advantages to the development of LIG in glasses. Glasses, compared to crystalline materials, are easier to manufacture and shape. In addition, the manufacturing costs are less than the costs of crystalline materials. The possible devices that can be realized include holographic devices, holographic narrow-band rejection filters (notch filters), optical demultiplexers, random-access memory (RAM), and read-only memory (ROM) [6].

Four-wave mixing experiments with aluminosilicate glass have shown an increase in laser-induced gratings as a function of increasing europium dopants [A.Y. Hamad

private communications]. Migration of ions, such as sodium, is believed to be the reason for the formation of laser-induced gratings. It has been proposed that migration is driven by the phonons emitted from the nonradiative relaxation of the europium ions [27]. The activation energy that can be gained from ionic conductivity studies may help understand the dynamics of the proposed ion hopping in FWM experiments.

This research is a continuation of previous work done in ref. [6]. The ionic conductivity of aluminosilicate glass is measured as a function of increasing europium dopants. The conductivity is also measured as a function of increasing sodium content. A comparison of the effects in varying europium and sodium concentration will be made. The frequency characteristics are also presented in the modulus, dielectric, and loss-angle formalism. In order to properly present the experimental data, the theory in atomic structure of glass, ionic conductivity, and impedance spectroscopy will be discussed briefly. A summary of impedance measurement techniques will also be discussed.

1.1 Structure of Silicate (SiO₂) Glass

Non-crystalline dielectrics are referred to as either amorphous or glassy. Amorphous materials can be prepared by a variety of techniques, for example, vacuum deposition, cooling from the melt, or sol-gel methods. The term “glass” is often restricted to amorphous materials prepared by cooling from the melt. The properties of both non-crystalline solids are similar. Unlike crystalline solids, amorphous or glass materials exhibit a short-range order but lacks long-range order. For instance, silicate glasses (SiO₂) with atomic distances of 3.6 Angstroms exhibit short-range order at distances of

less than 10 Angstroms [1]. The main glass forming oxides are SiO_2 , B_2O_3 , GeO_2 and P_2O_5 . The compositions of glass consist of various materials with different types of bonding. The typical bonds that form glass includes covalent (SiO_2), ionic ($0.4\text{Ca}(\text{NO}_3)_2-0.6\text{KNO}_3$), metallic ($0.4\text{Fe}-0.4\text{Ni}-0.14\text{P}-0.06\text{B}$), van der Waals (toluene), and hydrogen (H_2O) [2]. This study is concerned only with silicate glasses (covalent).

Vitreous silica has many of the structural features of more complex silicate glasses. To understand the structure of vitreous silica, we first consider the short-range structure. The radial distribution function (RDF) data obtained from x-ray diffraction, gives forth evidence that vitreous silica forms a tetrahedral structure, since the values from the RDF correspond to that of crystalline SiO_2 , which has already been established to have a tetrahedral formation [10, 12]. The RDF from x-ray scattering is shown in figure 1.0a. The peak at 1.6Å is the bond length between Si-O adjacent atoms. The peak at 2.6Å represents the distance between the neighboring oxygen atoms (O1, O2, O3, and O4 from figure 1.0b) that are attached to the same silicon central atom. The 2.6/1.6 ratios suggest a bond angle of 109 degrees between the O-Si-O. The peak at 3Å arises from the adjacent tetrahedral Si1-Si2 central atoms (figure 1.0b). The peak at 4Å represents the silicon to oxygen distance from adjacent tetrahedra. The uncertainty of the atomic positions becomes evident at larger separations due to the broad RDF [10]. Therefore, a spread of distances between Si central atoms of the tetrahedra exists and is consistent with the CRN model established by Zachariasen [12].

The structural details derived from the RDF do not give a precise geometry of the long-range structure of glass. In 1932, W.H. Zachariasen, in his paper "The Atomic Arrangement in Glass", established what is known as the continuous-random-network

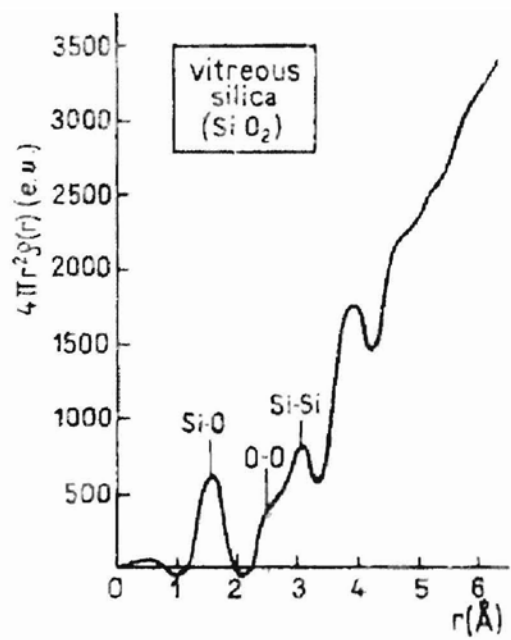


Figure 1.0.a

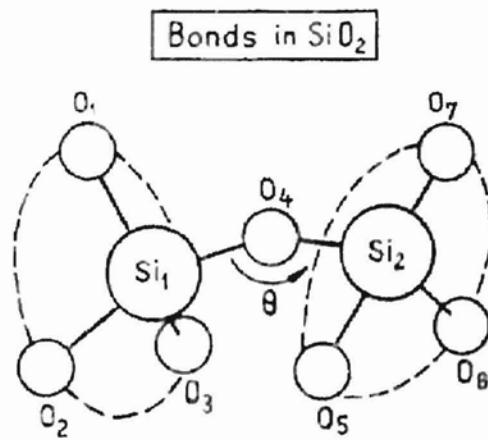


Figure 1.0.b

model (CRN) of covalently bonded amorphous solids [2, 11]. The CRN model is summarized as follows [1,2, 6, 11,12]:

1. Each oxygen atom is linked to no more than two cations.
2. The oxygen coordination number of the network cation is small.
3. The coordination polyhedron formed by oxygen atoms share only corners and not edges or faces.
4. At least three corners of each oxygen polyhedron must be shared in order to form a three-dimensional network
5. The sample must contain a high percentage of network cations, which are surrounded by oxygen tetrahedral or triangles.
6. The tetrahedral or triangles share only corners with each other.
7. Some oxygens are linked only to two network cations and do not form further bonds with any other cations.

The last three rules are added modifications to the rules of Zachariasen. To describe glass-network formation, Zachariasen added that the long-range disorders in glasses are results from the variations in bond lengths or bond angles, and the rotation about the axes of structural units such as the SiO_4 polyhedron. For instance, the broadening of the peaks (figure 1.0a) as the interatomic distances are increased suggests a spread of corresponding distances in glass, which is consistent with the CRN model [12].

Rules 1, 3, and 4 make it possible to have a three-dimensional tetrahedra structure with long-range disorder. The silicon is the network forming cation in this case, and the oxygen is tetrahedrally bonded to the silicon. Thus, the silica glass-formation consists of

corner sharing SiO_4 tetrahedra and each oxygen is bonded to only two silicons. With this formation, it is possible to have an open structure in which the Si-O-Si angle may vary without distorting the SiO_4 tetrahedra. Going back to figure 1.0, the first two peaks at 1.65Å and 2.65Å are narrow which suggest that distances are constant in the silica glass; hence, the tetrahedra are not distorted [12]. The angle between both tetrahedral (figure 1.0b) varies in angle from 120 to 180 degrees with a distribution maximum at 144 degrees [11]. Therefore, with rules 1, 3, and 4, a three-dimensional tetrahedral structure with long-range disorder is possible [12].

Rule 2, which is closely related to rule 1, merely gives the silicon coordination number of four. Since the coordination numbers of the different atoms are interdependent, this leads to the oxygen coordination number of two. Figure 1.1 gives a two-dimensional cartoon of the vitreous silica network. Note that a fourth oxygen is understood to be above each silicon central atom. The smaller solid black circles represent the silicon central atom while the larger open circle represents the oxygen atom. There is an apparent set of rings consisting of three or more tetrahedra characterized by interstices with varying sizes and shapes [11, 12].

The oxides of the alkali and alkaline earth elements alone do not form glasses. Even though the oxides do not form glasses, the structure of silicate glasses to which they are added still depends on the addition of Na_2O , and MgO network modifying oxides (NMO). When NMO's are added, the SiO_2 network breaks the Si-O-Si bonds resulting in the formation of non-bridging oxygens (NBO) that are electronegative in nature. Each NBO maintains charge neutrality nearby Na^+ , and Mg^{2+} ions. Figure 1.2 is a two-dimensional illustration of the silicate glass with network-modifying ions (NMI).

Figure 1.1 – Schematic of SiO_2 glass network (after ref. 6)
An oxygen atom is understood to be located above each Si^{4+} cation.

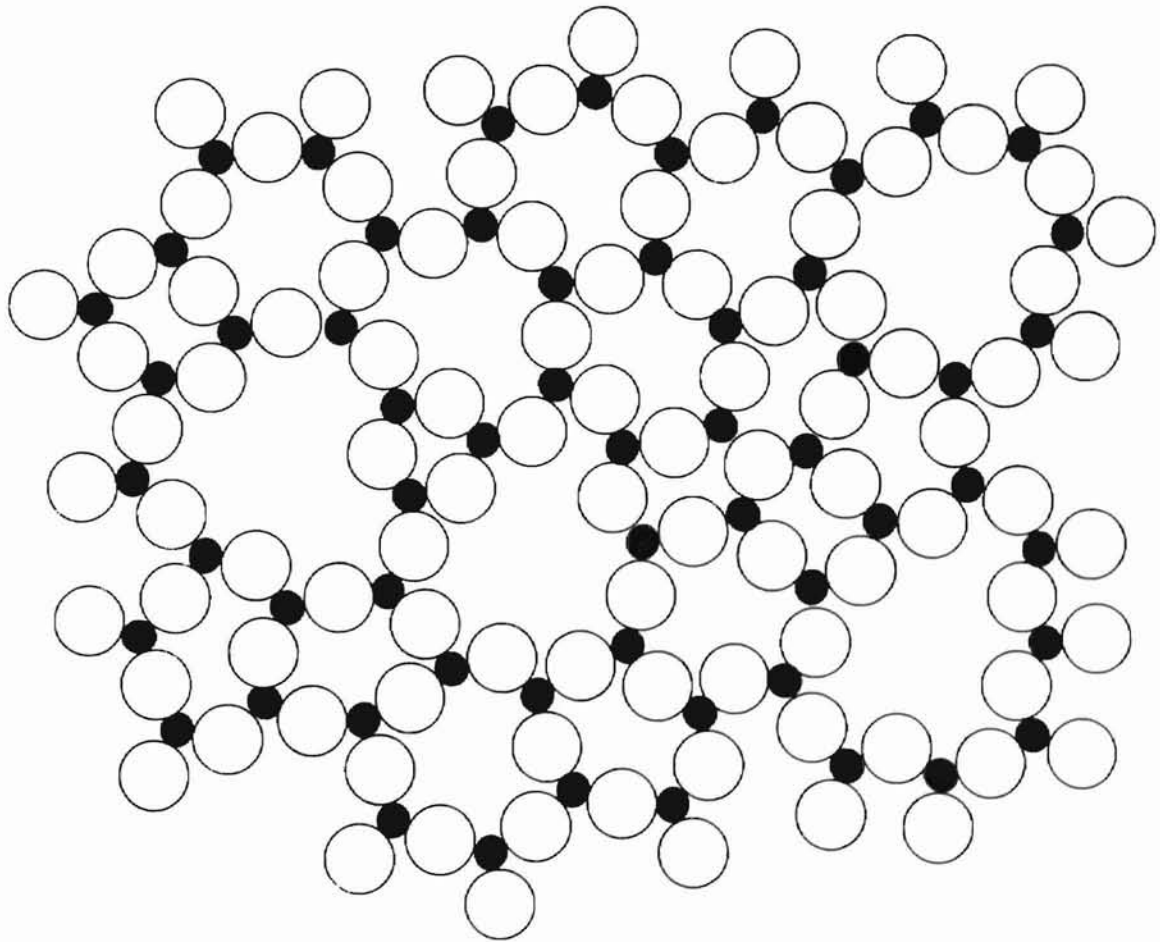
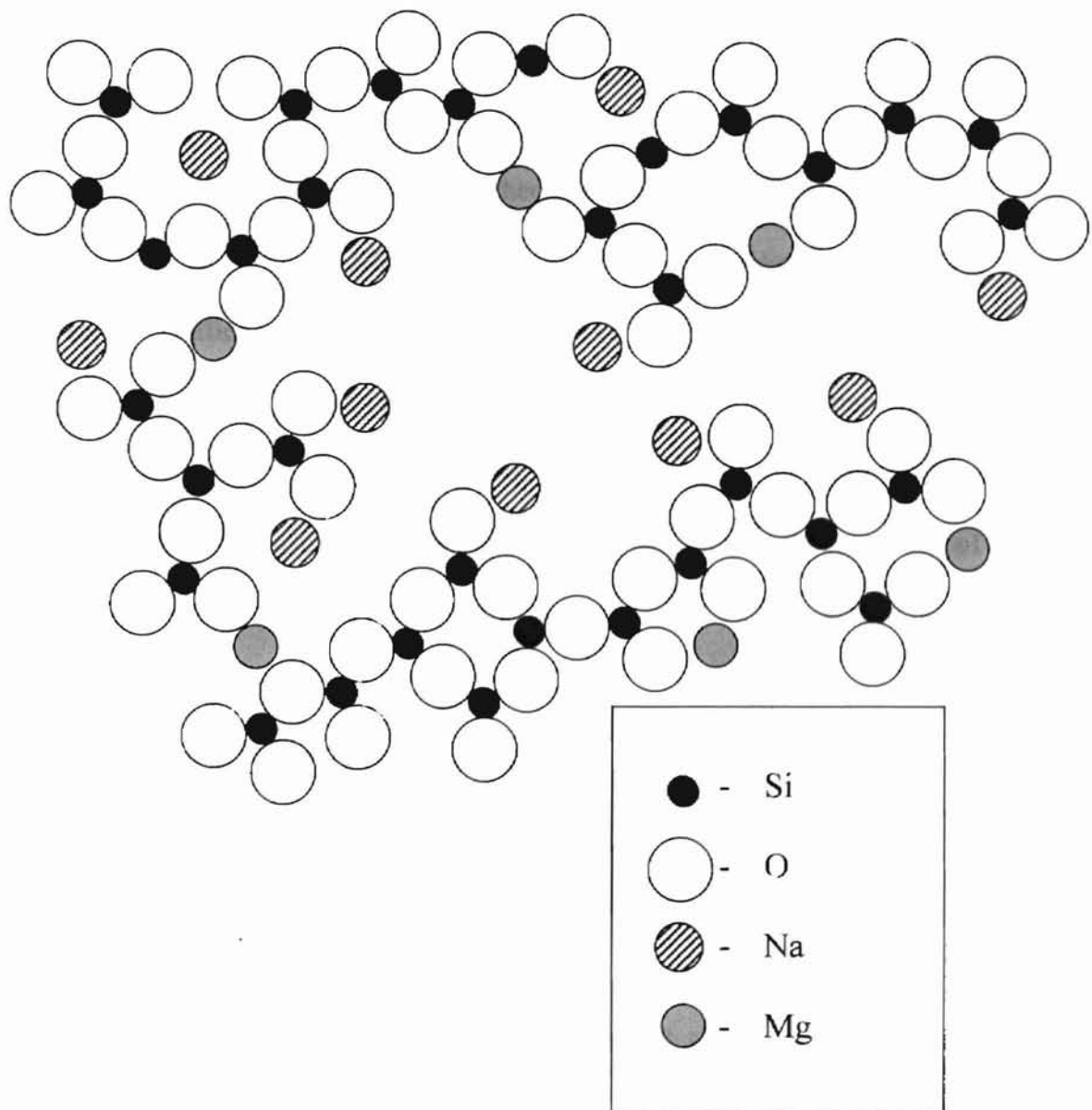


Figure 1.2 – Schematic of modified SiO_2 network (after ref. 6)

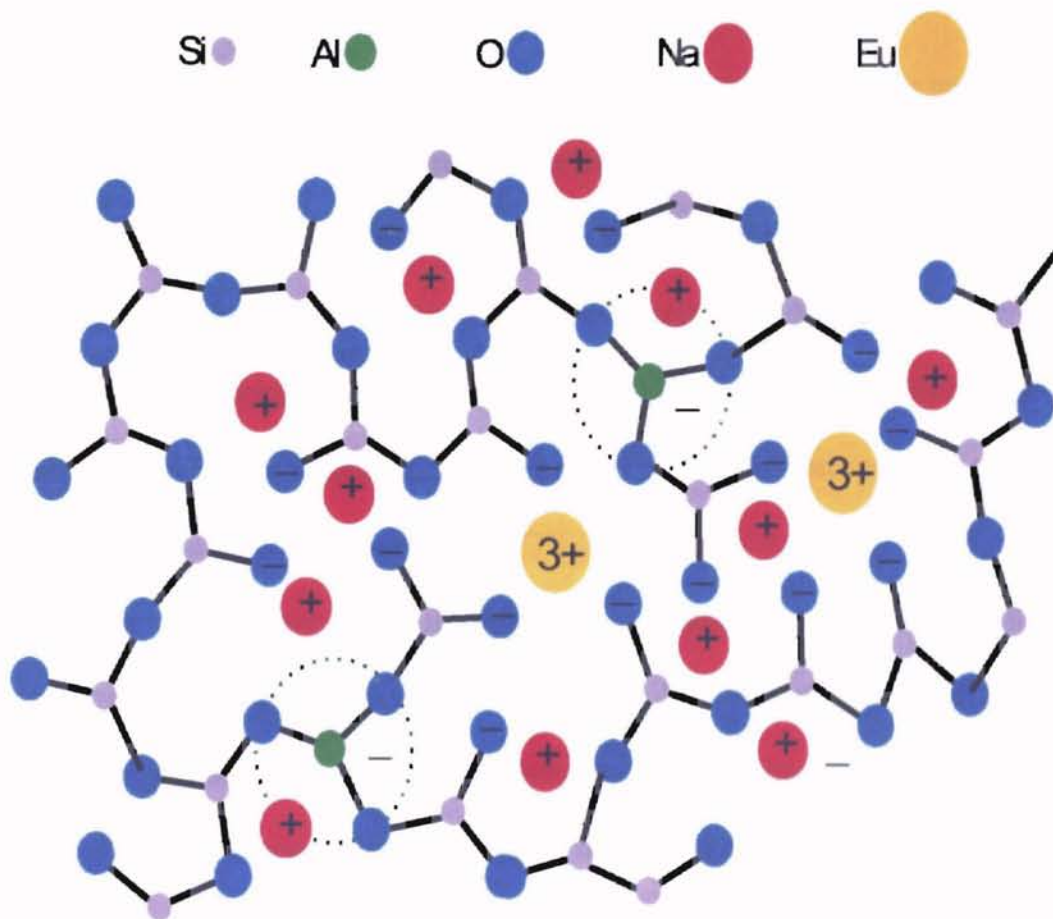


From the illustration, the Mg^{2+} ions charge compensates twice as many NBOs as the Na^+ ion. In general, alkali ions bonds to one NBO, and alkali-earth ions bonds to two NBOs. The bonds between the NMI and NBO are mostly ionic and are considered weaker than the covalent Si-O bonds [6]. As a final note, the Mg^{2+} modifiers have a stronger linkage to the NBOs compared to Na^+ modifiers which means alkali earth modifiers are less mobile than alkali modifiers. As a result, the addition of alkali earth modifiers reduces the ionic conductivity but at the same time improves the durability of the glass structure [11].

Figure 1.3 is a two-dimensional schematic of aluminosilica glass with Eu^{3+} dopants. Note that the Mg^{2+} NMI is not incorporated in this picture for simplicity. Rare-earth oxide modifiers, such as Eu_2O_3 , break the Si-O bonds resulting in three NBOs with Eu^{3+} for charge compensation. Much like the Mg^{2+} , the addition europium oxides inherently reduce the Na oxides, and the Eu^{3+} ions are more tightly bound by three NBOs. In addition, alkaline earth and rare-earth modifiers occupation in the interstices of the glass network may tend to block the mobile ions [14]. Therefore, a decrease in conductivity is expected.

The Al_2O_3 oxide is a glass former in this case (figure 1.3). It is well established that (AlO_4) aluminum forms into tetrahedra coordination in crystals. In glass, the aluminum-oxygen tetrahedra can only occur if the concentration of alkali or earth alkaline oxides is equal or greater than the concentration of aluminum oxides. If the Aluminum concentration exceeds the concentration of alkali or earth alkaline oxides, this model is not ideal since this results in the lack of cations for charge compensation. Aluminum by itself is not a glass-former, but substitution into vitreous silica will result in the aluminum

Figure 1.3: Aluminosilicate glass with Eu^{3+} dopants (after ref. 7)



replacing the silicon glass former. The AlO_4 tetrahedra have an overall negative charge [11]. This excess negative charge is compensated by a Na ion (figure 1.3). The Na ions close to the AlO_4 structure have less binding energy in comparison to the Na ions bound to NBOs. Therefore, it is expected that an increase in Al_2O_3 oxides will increase ionic mobility. Previous studies have actually shown that an increase in Al_2O_3 substitution also increased ionic conduction [6].

As a final note, each aluminum oxide only provides 1.5 oxygens per aluminum-oxygen tetrahedron, which is insufficient for the 2.0 oxygens per tetrahedron requirement. This requirement is satisfied by oxygens from the alkali or earth-alkaline oxides. Therefore, each Aluminum substitution reduces the NBOs in the glass network such that when the concentration of aluminum equals the NBOs, the structure will become a fully linked network with no NBOs. Total connectivity of the glass network will occur when the molar concentration of aluminum is 27% [6].

For a quantitative model, the Q_n notation is commonly used to express the concentration of bridging oxygens per tetrahedron. The subscript n is the number of bridging oxygens. A tetrahedron that is fully linked to four bridging oxygens is referred to as a Q_4 . Tetrahedrons with three bridging oxygens and one non-bridging oxygen is referred to as a Q_3 unit, and so forth. In the vitreous silica model, the SiO_4 tetrahedron is a Q_4 . Addition of Na_2O oxides replaces each Q_4 species with Q_3 species. Finally, addition of MgO oxides replaces each Q_4 species with two Q_3 species. This continues until all Q_3 species has replaced the Q_4 species. Additional increase of NBOs at this point will replace Q_3 species with Q_2 species, and so forth [6]. Eu^{3+} oxides readily form Q_2 and Q_1 species [7].

1.2 Ionic Conductivity of Silicate Glass

The electrical properties of glass are dependent upon the ionic migration within the glass network. The electrical properties of inorganic glass are mainly due to the migration of monovalent ions, such as Na^+ , under the influence of an electric field. Under an alternating electric field, the ionic migration, both long-range and short-range, is often the cause of dielectric losses. Ionic mobility is quantitatively expressed in terms of the conductivity of the glass network.

Ionic conductivity in glasses is a thermally activated hopping process across an energy barrier. Figure 1.4 is an illustration of a linear potential well. This illustration assumes only one type of mobile ion is trapped in a potential well. The potential well arises from the glass network (Note that figure 1.4 illustrates the average barrier potential in which an ion experiences, but later, a discussion on barrier potentials with varying heights will be presented). Under zero electric field, the ion has an equal probability of jumping in any direction resulting in zero net motion or net current flow. At absolute temperature, T , the probability per second that an oscillating ion overcomes the potential barrier, ϕ , is given by, $\nu \exp(-\phi/(k_b T))$, in which ν represents the oscillation of the ion (10^{12} to 10^{13} Hz) in its interstices. The constant k_b is Boltzmann's constant [12].

When an electric field, E , is applied, the shape of the potential well is modified as shown in figure 1.4b. The work done by the electric field on the ion is, eEd , where e represents the charge of the ion, and d is the separation of the adjacent sites of lowest energy. The process of ion hopping is not usually instantaneous, even at the presence of

Figure 1.4.a – Periodic potential wells (after ref. 6)

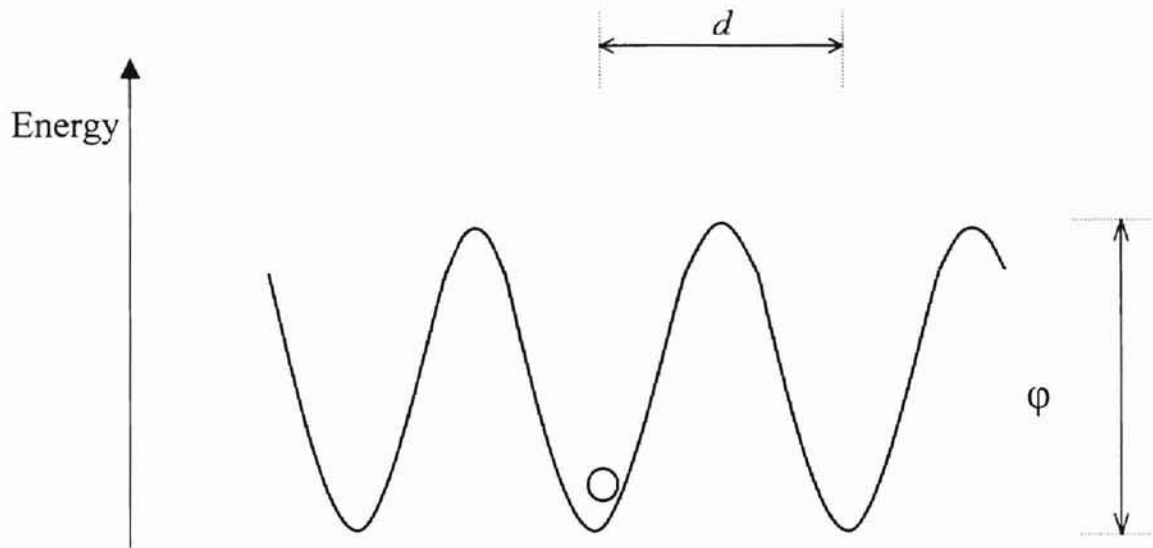
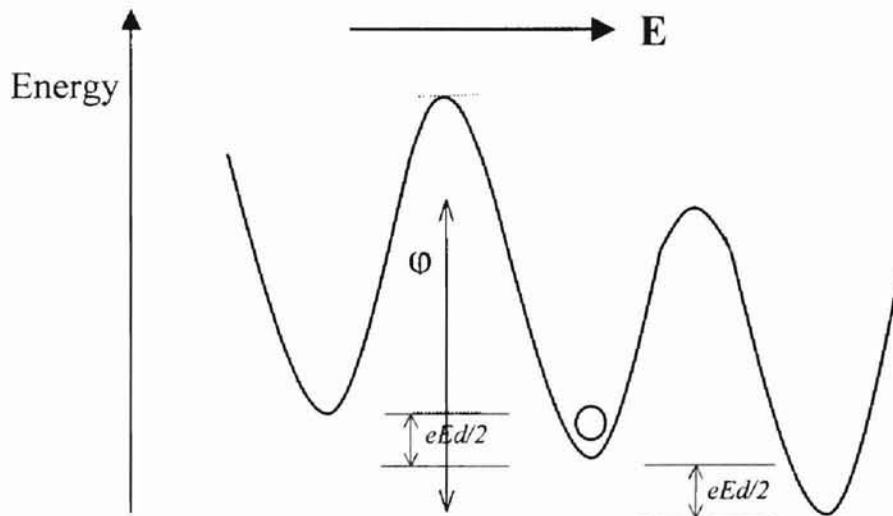


Figure 1.4.b – Periodic potential wells in the presence of an electric field (after ref. 6)



an electric field. At certain temperatures, the ions may not have enough energy gain to hop a potential barrier. The ions gain the extra energy by collisions with other thermally excited ions. A distribution of elapsed time is associated for each ion gaining the thermal energy. The mean value of such elapse time is referred to as the relaxation time constant, τ . In other words, the probability of an ion hop after an elapse time τ is usually defined as an exponential $P(t) = P_0 (1 - e^{-t/\tau})$ [15].

The energy barrier closer to the positive electrode is slightly increased by $+eEd$. On the other hand, the energy barrier closer to the negative electrode is slightly reduced by $-eEd$. Thus, the energy barrier experienced by an ion that is in the same direction as the electric field and against the electric field is given by $(\phi - e E d/2)$ and $(\phi + e E d/2)$, respectively. The net probability for ions “flowing” with the electric field is then given by

$$\begin{aligned}
 P &= v (P_+ - P_-) \\
 P &= v \exp(-(\phi - e E d/2)/(k_b T)) - v \exp(-(\phi + e E d/2)/(k_b T)) \\
 &= v \exp(-\phi/(k_b T)) [\exp(e E d/(2k_b T)) - \exp(-e E d/(2k_b T))]
 \end{aligned}$$

Note that eEd is much less than $2k_b T$ in these types of experimental conductivity measurements. This approximation is valid from room temperature to field strengths of about 10 V/cm. Applying the power series on the net probability equation and keeping only the first two terms due to the $eEd \ll 2k_b T$ approximation, the probability equation simplifies as follows:

$$\begin{aligned}
 P &= v \exp(-\phi/(k_b T)) [1 + eEd/(2k_b T) - (1 - eEd/(2k_b T))] \\
 &= v [eEd/(k_b T)] \exp(-\phi/(k_b T)).
 \end{aligned}$$

The mobile ions have a mean velocity, $u = P d$. The mobility is given by $\mu = u / E$. At

weaker fields, the current and field strength are proportional which also satisfies Ohm's Law. In this case, the current density is given by $I = N e u$, where N is the volume density of the migrating ions. Plugging in the all the values,

$$\begin{aligned} I &= N e P d \\ &= N e d v [e E d / (k_b T)] \exp(-\phi / (k_b T)) \\ &= [(N v E e^2 d^2) / (k_b T)] \exp(-\phi / (k_b T)). \end{aligned}$$

The conductivity is then given by $\sigma = I / E$, therefore

$$\sigma = I / E = [(N v e^2 d^2) / (k_b T)] \exp(-\phi / (k_b T)).$$

To derive the Arrhenius equation, the above expression is multiplied by the absolute temperature T , thus

$$\sigma T = A \exp(-\phi / (k_b T))$$

where $A = (N v e^2 d^2) / (k_b T)$ [6, 12, 13].

The potential barrier parameter, ϕ , in this case represents the dc conductivity activation energy. The experimental Arrhenius plot is normally linear, and the activation energy is derived by determining the plot slope. The temperature dependence is nearly constant on certain ranges; however, the activation energy has temperature dependence from 323 K through the glass transition temperature [6]. Below 323 K, surface conduction will cause deviations to the conductivity data. Typical activation energy values range from 0.55 and 1.1 eV [15]. According to the *Anderson and Stuart model (1954)*, the activation energy, ϕ , is a sum of two independent terms, the *electrostatic binding energy*, E_b , and the *strain energy*, E_s . E_b is the energy required to break the local bond, and E_s is the energy required to move the ion to the next interstice. The expressions for both terms are as follows,

$$E_b = (\beta z z_o e^2) / (\gamma (r + r_o))$$

$$E_s = 4 \pi G r_d (r - r_d)^2.$$

The β parameter is the distance between neighboring sites. The charge of the cation and anion are z and z_o respectively. The radius of the cation and anion are r and r_o , respectively. The covalency parameter, γ , measures the deformability of the anion, and experimentally comparable to the dielectric constant of the glass. The factor, G , gives the shear modulus of the glass network. Last, r_d is the distance between interstices. The representation of the activation as a sum of two independent terms has remained unchallenged. An increase in the Na₂O content affects the conductivity in the following ways. First, the increase in Na⁺ ions reduces the lattice parameter β , since cation sites are moving closer to each other. Second, an increase in the polarizability of the oxide ions results in an increase in the covalency parameter γ . Last, an increase in NBOs reduces the rigidity of the glass network, and increases the number of interstices, resulting in an increase in the parameters, G and r_d [5, 6, 13]. Further details of glass structure with respect to ionic transport activation energies can be found in ref. [24].

The pre-exponential factor, A , includes a constant, $1/3 - 1$, to account for the number of ways a mobile ion may jump in three-dimensional space [6]. There are discussions on the dependence between A and E (Ruetschi 1958, et al); however, it is unimportant in the discussion of the electrical properties of glass [13]. In addition, the contribution of the pre-exponential factor to the ionic conductivity is negligible compared to the contribution of the activation energy, at fixed temperatures [6].

The discussion on ionic conductivity up to this point has assumed a non-alternating electric field, and potential barriers of the same magnitudes. The model for ac

conduction in this study follows Stevels [ref. 15] random potential energy barrier. For a discussion of other models, see the article by Dyre [ref. 19].

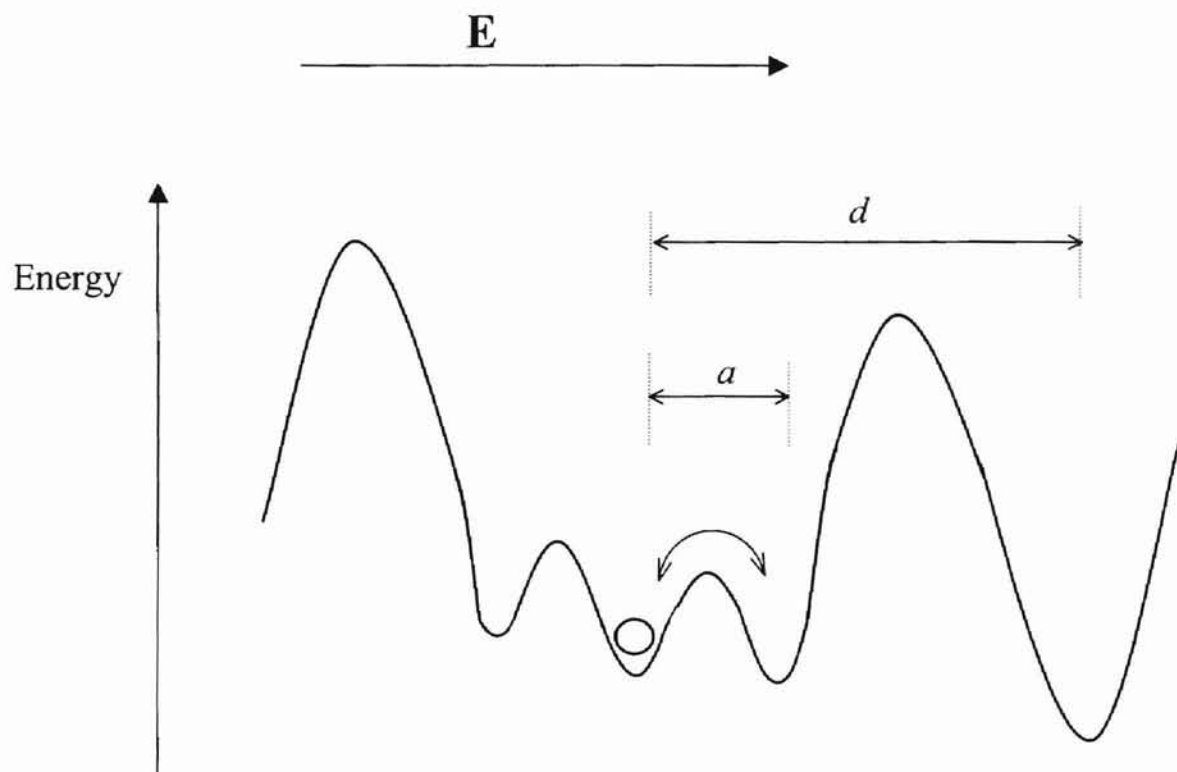
Under an alternating electric field, $E_o \exp(i\omega t)$, the conductivity has both temperature and frequency dependence. The ideal potential barrier in a random glass network, as shown in figure 1.5, consists of smaller potential wells, separated by a mean distance a , inside larger potential wells, separated by a mean distance d . As discussed previously, the effect of an electric field will again increase or decrease the barrier by eEd for the larger potential, and by eEa for the smaller potential wells. The probability of an ion hopping in the smaller energy barriers is more likely to occur compared to an ion hop of the larger energy barriers. Therefore, an ion will immediately gain enough thermal energy to hop the small barriers, in an elapse time of τ_{ac} . The elapsed time required to hop the larger barrier will be referred to as τ_{dc} . In the glass network, there are distributions in height and distances for the potential barriers; therefore, a distribution of relaxation times is expected [6,15].

When the frequency of oscillation, ω , of the electric field is comparable to $1/\tau_{ac}$, and less than $1/\tau_{dc}$ by default, the direction of the ion hopping will correspond to the oscillation of the electric field. The ions will then gain energy, which transmit to the glass network, as dielectric losses. This type of loss is referred to as conduction losses. Additionally, the ac conductivity will have larger values compared to dc conductivity measurements. The ac conductivity in this case can be described by a power-law dependence over a range of frequency, which is approximated by [5,6,19]:

$$\sigma_{ac}(\omega) = \sigma_{dc} + B \omega^n$$

where n is approximately unity.

Figure 1.5 – Hypothetical potential wells (after ref. 6)



If the magnitude and frequency are reduced ($\omega \ll 1/\tau_{dc}$), the dc conductivity and ac conductivity are equivalent ($\sigma_{ac}(\omega) = \sigma_{dc}$) since the direction of the field only changes in every few seconds. Suppose the instantaneous electric field strength is close to zero with $\omega \ll 1/\tau_{dc}$, then an ion hop still occurs with minimal energy and losses. Nevertheless, if ω approaches the value of $1/\tau_{dc}$, then the ions, on the average, will only hop when the instantaneous electric field strength reaches maximum; therefore, the ions gain considerable energy resulting in large losses. This is referred to as migration losses. Typically, the losses described are a result of the hopping ions losing energy into the glass network, in the form of heat [5,6,15].

1.3 Impedance Spectroscopy

Virtually all materials such as solids and liquids are able to pass a charging current when a voltage is applied across the materials. If the applied voltage is constant (dc), then the ratio of the voltage to the current (V/I) is referred to as the resistance of the material. If the applied voltage is varying (ac), then the ratio of the voltage to current ratio (V/I) is referred to as the impedance of the sample. Due to the physical properties of solids or liquids, the impedance is frequency dependent. Therefore, Impedance spectroscopy is an ac measurement method used to obtain physical and chemical characteristics of electrolytic liquids and solid materials. The advantages of impedance spectroscopy are the accurate and repeatable acquisition of measurement, and the process

is non-destructive. Additionally, there are wide ranges of systems that can be analyzed, i.e. battery systems, frequency response of electrical circuits, analysis of organic tissues, etc. In this experiment, the usefulness of impedance spectroscopy is that the dc resistance of the electrode-material interface can be measured [6,16].

In general, the method of characterization is by means of an electrical analog, such as a circuit-equivalence of the electrode-material interface. A circuit model has already been established from previous studies, as illustrated in figure 1.6.a, and 1.7.a [after ref. 6]. The equivalent circuit element consists of a parallel RC pair (R_b and C_o), and in series with a capacitor (C_{dl}). The circuit element R_b is the dc resistance (bulk resistance) of the glass sample, C_o is the vacuum capacitance of the electrode-electrode cell, and C_{dl} is the double-layer capacitance. The double-layer capacitance is from a build-up of ions in the electrode-material interface. The build-up forms because the negatively charged electrode attracts the positively charged mobile ions to the electrode surface. The separation between the electrode-ion layers is in the order of angstroms. The resulting layers of electrode-ions is analogous to a parallel plate capacitor, hence C_{dl} is in series [18]. The double-layer capacitor tends to cause a potential drop. The corresponding Nyquist plot is shown in 1.6.b, and 1.7.b for the RC parallel circuit, and the RC parallel circuit in series with C_{dl} . The plot has a parametric parameter in ω , and appears to form a semi-circle as ω is increased.

When an alternating voltage source, $V = V_o e^{j\omega t}$, is applied across an ideal capacitor with vacuum as its dielectric, a resulting alternating current $I = I_o e^{j(\omega t - \phi)}$ will charge the capacitor. This current lags the voltage by a phase angle of $\phi = \pi/2$. Note that if the circuit model were an inductor, the current will lead the voltage by $\phi = \pi/2$.

Figure 1.6.a – RC pair circuit

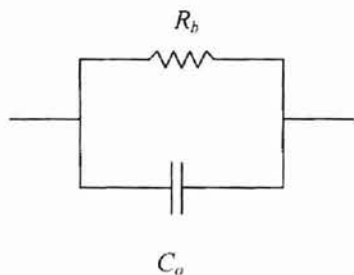


Figure 1.6.b – Impedance plot of RC pair

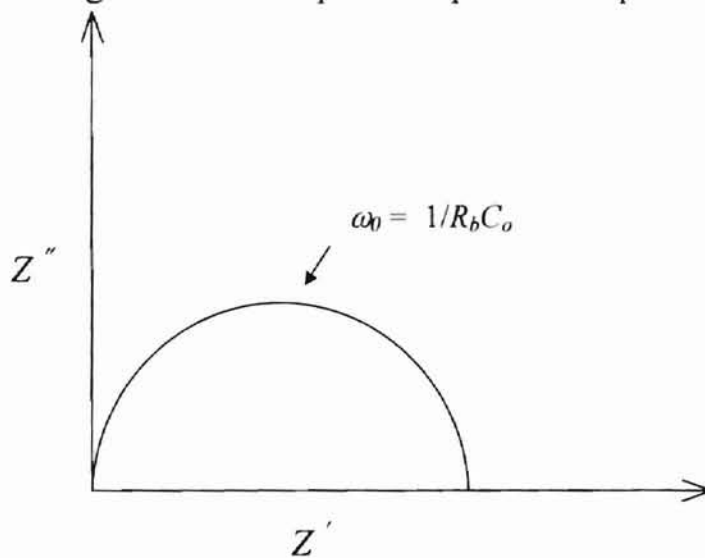


Figure 1.7.a – RC pair in series with capacitor

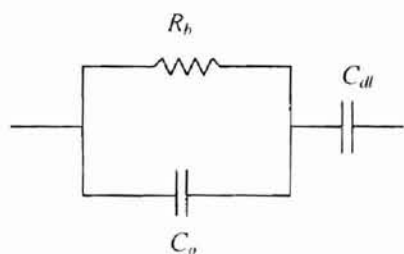
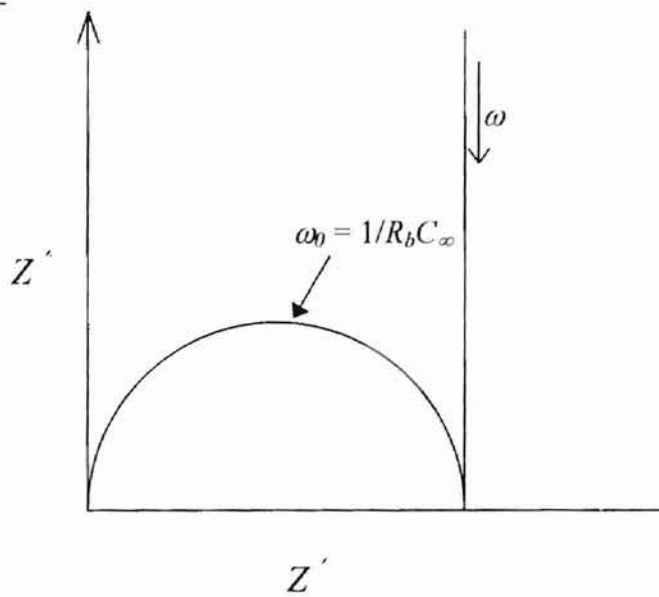


Figure 1.7.b – Impedance plot of RC pair in series with capacitor



The charge stored in such a system is $Q = C_o V$. C_o is the vacuum capacitance, given by $C_o = A\epsilon_o/d$ farads, where A is the area of the parallel plates, d is the distance between the parallel plates, and ϵ_o is the permittivity of free space. If a dielectric solid is present, the capacitance is increased by a factor of ϵ^* , thus, the total capacitance is $C = \epsilon^* C_o$. The charge stored in such a system is then given by $Q = C V$. The impedance is then calculated by $Z = V/I$,

$$\begin{aligned} Z &= (V_o e^{i\omega t}) / (I_o e^{i(\omega t - \phi)}) \\ &= Z_o e^{i\phi} \end{aligned}$$

where $Z_o = V_o / I_o$. Using Euler's relationship, $\exp(ix) = \cos x + i \sin x$, the impedance expression becomes,

$$\begin{aligned} Z &= Z_o e^{i\phi} \\ &= Z_o (\cos \phi + i \sin \phi). \end{aligned}$$

Hence, the impedance is separated by its real and imaginary parts, $Z = Z' - i Z''$, where $Z' = Z_o \cos \phi$, and $Z'' = Z_o \sin \phi$ [17].

The impedance of the circuit model (figure 1.6) is derived using Ohm's Law, $Z_{tot} = Z_{dl} + Z_{rc}$, where Z_{dl} represents the impedance of the double layer capacitance, and Z_{rc} is the impedance of the parallel RC circuit. From circuit theory, the impedance of the parallel RC circuit is given as $Z_{rc} = Z_C R_b / (Z_C + R_b)$, where Z_C represents the frequency dependent impedance of a capacitor (*capacitive reactance*). The frequency dependence of the capacitor elements is determined by starting with $I = dQ/dt$ [17]:

$$\begin{aligned} I &= (d/dt) (C V) = \epsilon^* C_o (d/dt) (V_o e^{i\omega t}) \\ &= i\omega \epsilon^* C_o V_o e^{i\omega t} = i\omega \epsilon^* C_o V. \end{aligned}$$

The impedance of the capacitor can be obtained by comparing the above expression to

Ohms relation $V = I Z_C$; hence, we get the expression $Z_C = 1 / i\omega\epsilon^* C_o = 1 / i\omega C$ for the capacitive reactance of any capacitor. Given the capacitive reactance, the total impedance of the circuit model is obtained by substitution and “rationalizing” the denominators, appropriately:

$$\begin{aligned}
 Z_{tot} &= (1 / (i\omega C_{dl})) + Z_C R_b / (Z_C + R_b) \\
 &= (1 / (i\omega C_{dl})) + (R_b / (i\omega C_C)) / (R_b + 1 / (i\omega C_C)) \\
 &= (-i / (\omega C_{dl})) + (R_b / (1 + i\omega C_C R_b)) \\
 &= (-i / (\omega C_{dl})) + (R_b - i\omega C_C (R_b)^2) / (1 + (\omega C_C R_b)^2) \\
 &= [R_b / (1 + (\omega C_C R_b)^2)] \\
 &\quad -i [1 / (i\omega C_{dl}) + (1 / \omega C_C (R_b)^2) / (1 + (\omega C_C R_b)^2)].
 \end{aligned}$$

In the limit $\omega \ll 1$, the real component of Z_{tot} approaches R_b (Bulk or dc resistance) and the imaginary component approach infinity [6]. The Nyquist plot in figures 1.6.b and 1.7.b illustrates the behavior of the impedance circuit model. The plot is characterized by a semi-circle. The imaginary component in this plot approaches infinity as the frequency of the oscillating source approaches zero.

Real world data Nyquist plots, however, usually results in a flattened or depressed semi-circle with the center being below the real axis. The most common explanation is that there’s some property of the system that is inhomogeneous, or there may be a distribution of some physical property in the system. Another possible explanation is the smoothness of the samples surface, and also the electrode plating may have varying thickness. This inherent annoyance is modeled by assuming the dc resistance is in parallel with a constant phase element (CPE). Mathematically, the impedance of the CPE is $1/Z = Y = Q^o (i\omega)^n$, where $0 \leq n \leq 1$. The CPE has an impedance value of $-(90 * n)$ and

its independent of the frequency. If $n=1$ the CPE behaves like an ideal capacitor.

Generally, the in-phase current and the resistive element of such an RC response is represented by using a complex impedance $\epsilon^* = \epsilon' - i \epsilon''$. The real part represents the instantaneous polarization due to electron displacement. The imaginary part represents the polarization that is 90 degrees out of phase due to the long range and short-range migration of ions. The current expression then becomes,

$$\begin{aligned} I &= i\omega (\epsilon' - i \epsilon'') C_o V \\ &= \omega \epsilon'' C_o V + i\omega \epsilon' C_o V \\ &= I_L + I_C. \end{aligned}$$

The real component is referred to as the in-phase or loss current $I_L = \omega \epsilon'' C_o V$, and the imaginary component is referred to as the charging current $I_C = i\omega \epsilon' C_o V$. It is often convenient to represent the performance of a dielectric through a convention in terms of its loss angle, δ , between the quadrature, or imaginary, component of the current and the magnitude of the current. The relationship in the complex plane between the charging current and loss current is derived by starting with the magnitude of the total current,

$$|I| = (|I_L|^2 + |I_C|^2)^{1/2}$$

and

$$\begin{aligned} \tan \delta &= |I_L| / |I_C| \\ &= (\omega \epsilon'' C_o V) / (i\omega \epsilon' C_o V) \\ &= \epsilon'' / \epsilon'. \end{aligned}$$

The expressions for the individual components of the complex dielectric, $\epsilon^* = \epsilon' - i \epsilon''$, is derived by using the admittance relation $(Z^*)^{-1} = Y = I/V$

$$\begin{aligned} 1/(Z' + i Z'') &= (\omega \epsilon'' C_o V + i\omega \epsilon' C_o V) / V \\ (Z' - i Z'') / (Z'^2 + Z''^2) &= \omega C_o (\epsilon'' + i \epsilon'). \end{aligned}$$

Collecting and equating imaginary and real terms separately, we get,

$$\epsilon' = (I / \omega C_o) Z'' / (Z'^2 + Z''^2)$$

$$\epsilon'' = (I / \omega C_o) Z' / (Z'^2 + Z''^2).$$

The complex conductivity is calculated by using the relation $\sigma = I / (A E)$, where the electric field is equal to $E = V/d$. Therefore,

$$\begin{aligned} \sigma &= I / (A E) \\ &= (\omega \epsilon'' C_o V + i \omega \epsilon' C_o V) / (A V / d) \end{aligned}$$

and using $C_o = A \epsilon_o / d$, we get the following:

$$\sigma = (\omega \epsilon_o \epsilon'' + i \omega \epsilon_o \epsilon').$$

The $Re[\sigma] = \sigma(\omega) = \omega \epsilon_o \epsilon''$ represents the dielectric conductivity which is the sum of all the long-range losses in the media. The dielectric ϵ'' represents all of the losses in the system. To find the short-range ac losses one subtracts $\sigma(0) / \omega \epsilon_o$ from the expression of ϵ'' above, however, this may reduce the precision of the dielectric data. The peaks of the frequency dependent dielectric data plot can be used to determine the relaxation time of a solid dielectric. Theoretically, the frequency dependence of the complex dielectric was described by the Debye equations:

$$\epsilon' = \epsilon_{\infty} + (\epsilon_s - \epsilon_{\infty}) / (1 + \omega^2 \tau^2)$$

$$\epsilon'' = (\epsilon_s - \epsilon_{\infty}) \omega \tau / (1 + \omega^2 \tau^2).$$

The parameters ϵ_s , and ϵ_{∞} , represent the dielectric constants at $\omega \rightarrow 0$ and $\omega \rightarrow \infty$, respectively. The peak represents single relaxation times. However in ionic conductivity, there is a distribution of relaxation times due to the varying energy barriers; hence, the dielectric loss features a broad peak and it does not correspond to the sharp peaks from the Debye equations [6, 17, 20]. A new way of introducing dielectric data is then

necessary.

In the field of ionic conductivity, it is more common to present the ac data by using the form of the electric modulus $M^* = I / \epsilon^*$. Substitution of the complex dielectric expression gives the following,

$$M'(\omega) = \omega C_o Z''$$

$$M''(\omega) = \omega C_o Z'$$

The advantage of the electric modulus is that there is no contribution to the double-layer capacitance to $M''(\omega)$, and the imaginary part also gives Debye-like peaks. The peaks, however occur at higher frequencies compared to the dielectric peak. Even though both peaks are not equal, the functional increase or decrease is proportional [6,19].

As a summary, the following expressions are of experimental importance:

$$\epsilon' = (I / \omega C_o) Z'' / (Z'^2 + Z''^2)$$

$$\epsilon'' = (I / \omega C_o) Z' / (Z'^2 + Z''^2)$$

$$M'(\omega) = \omega C_o Z''$$

$$M''(\omega) = \omega C_o Z'$$

$$\tan \delta = \epsilon'' / \epsilon'$$

$$\sigma = I / (A E)$$

$$\sigma(\omega) = \omega \epsilon_o \epsilon''$$

CHAPTER II

EXPERIMENTAL METHODS

2.1 Measuring Techniques

AC impedance measurements can be accomplished in two ways: 1) comparative measurements with lump circuits, 2) direct measurements using lock-in amplifiers. Before digital technology, dielectric permittivity was measured using lump circuits. At medium frequency ranges (1 to 20,000 Hz), lump circuits, such as the a.c. bridge was the easiest to implement. The AC bridge is based on the concepts of the Wheatstone bridge. Figure 2.0 shows the Wheatstone bridge circuit. The circuit elements R_1 and R_2 represent standard resistors, R_p is a potentiometer, and R_x is an unknown resistor to be determined. An ammeter, denoted by D , is attached between terminals A and B . To reach a balanced condition, R_p is adjusted until the current across terminals A and B is null. When the Wheatstone bridge is balanced, Kirchoff's circuit laws imposes the following conditions:

$$I_1 = I_p$$

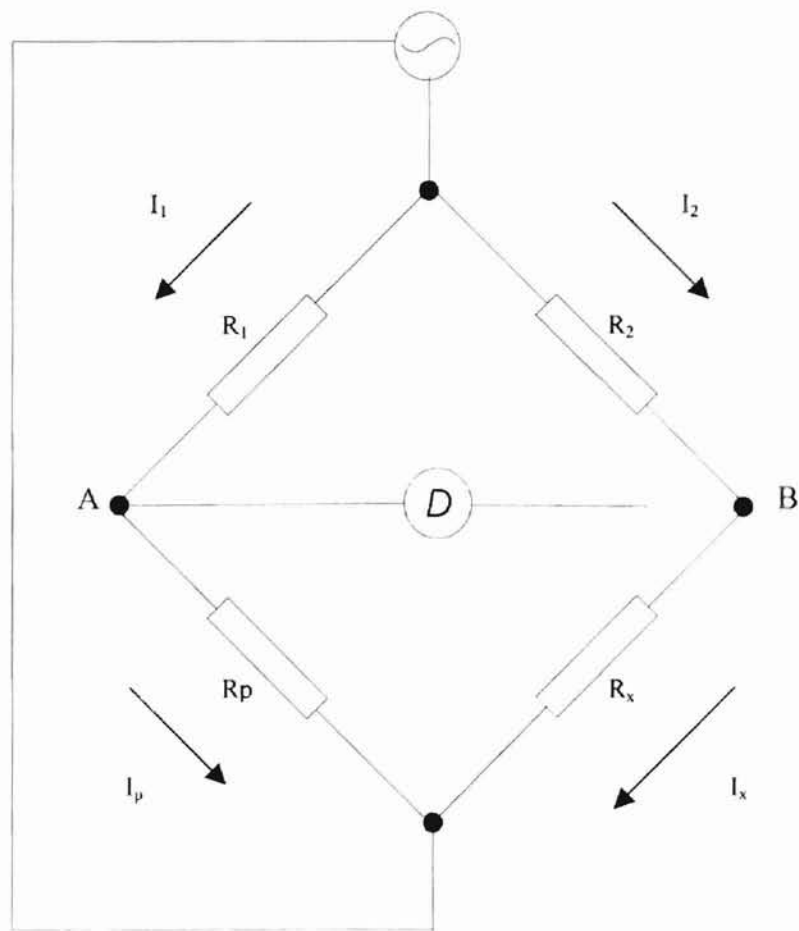
$$I_2 = I_x.$$

Since there is no current across the ammeter between terminals A and B , the voltage at both terminals are equal. Therefore, Kirchoff's voltage law holds:

$$V_A = V_B$$

$$I_1 R_1 = I_2 R_2$$

Figure 2.0: Basic Wheatstone Bridge



$$I_p R_p = I_x R_x.$$

Solving the four equations and four unknowns, the expression for the unknown value is therefore,

$$R_x = R_2 R_3 / R_1.$$

With ac bridges, the principles are similar ($V_A = V_B$), but the magnitude and phase must also equal. In addition, only a slight modification of figure 2.0 is required for a.c. bridges. Replacing the R_p potentiometer with a Z_p variable series resistance and capacitance, and taking $R_x \rightarrow Z_x$ to be the unknown impedance, the following equation holds true:

$$Z_x = R_2 Z_p / R_1$$

$$Z' = \text{Re} [Z_x] = R_1 R_p / R_2$$

$$Z'' = \text{Re} [Z_x] = (R_1 / R_2) / \omega C_p.$$

Other various lump circuits are used for other frequency ranges, and there is no single bridge equivalence to integrate all such lump circuits into a single equivalent circuit.

Additionally, bridge circuits require a vast learning curve to be effectively used, and may require long periods for impedance spectroscopy experiments [6, 16].

There are limitations at certain frequency ranges on a.c. bridges. The limit of higher frequency measurements is dictated by the non-linear nature of the impedance circuits and the effects of stray capacitance [16]. Bridge devices that utilize transformers as ratio arms may be used for higher frequencies; however, at low frequencies the cell current and voltage in a ratio arm bridge decreases with decreasing frequencies imposing a limit of around 100 Hz to 200 Hz. The null detection system used in a.c. bridges consists of an amplifier, filter, and a.c. voltmeter. The three components impose the

following low frequency limitations. At low frequencies, the experimental cell is more reactive thus the gain must be increased to detect the resistive component of the cell but may result in saturation of the detector. Analog filters for bandwidths below 10 Hz are not easily constructed and controlled; hence, significant source noise may result. These effects can be solved to some extent by using a lock-in amplifier [16].

The two inherent qualities of the lock-in amplifier is its ability to reduce noise (signal-to-noise ratio) and its ability to distinguish the phase-shift between the input and output. The essential component of a lock-in is the phase sensitive detector (PSD), which consists of a multiplexer and low-pass filter (time-averaging circuit). The multiplexer multiplies the input signal (V_i) with a reference signal (V_r). The reference signal (V_r) is used to excite the experiment resulting in an output (V_i) that is used as the input signal into the PSD. The Fourier component of the square-wave reference signal and input signal can be represented as follows:

$$V_r = (4/\pi) [\sin (\omega_r t) + (1/3) \sin (3\omega_r t) + (1/5) \sin (5\omega_r t) + \dots]$$

$$V_i = B \sin (\omega_i t + \theta)$$

where B is the amplitude of the input signal, and ω is the angular frequency. Note that the frequency generator of traditional analog lock-ins generates square-waves, whereas the more modern digital lock-ins generates sine waves. In practice $\omega_r = \omega_i$ since they are from a common source. The multiplexer output is then given by

$$\begin{aligned} V_{\text{mpx}} &= V_r V_i \\ &= (2B/\pi) [\cos (\theta) - \cos (2\omega_r t + \theta) + (1/3) \cos (-2\omega_r t + \theta) \\ &\quad + (1/3) \cos (4\omega_r t + \theta) + \dots]. \end{aligned}$$

When applied to the low-pass filter, the time dependent components goes to zero, hence

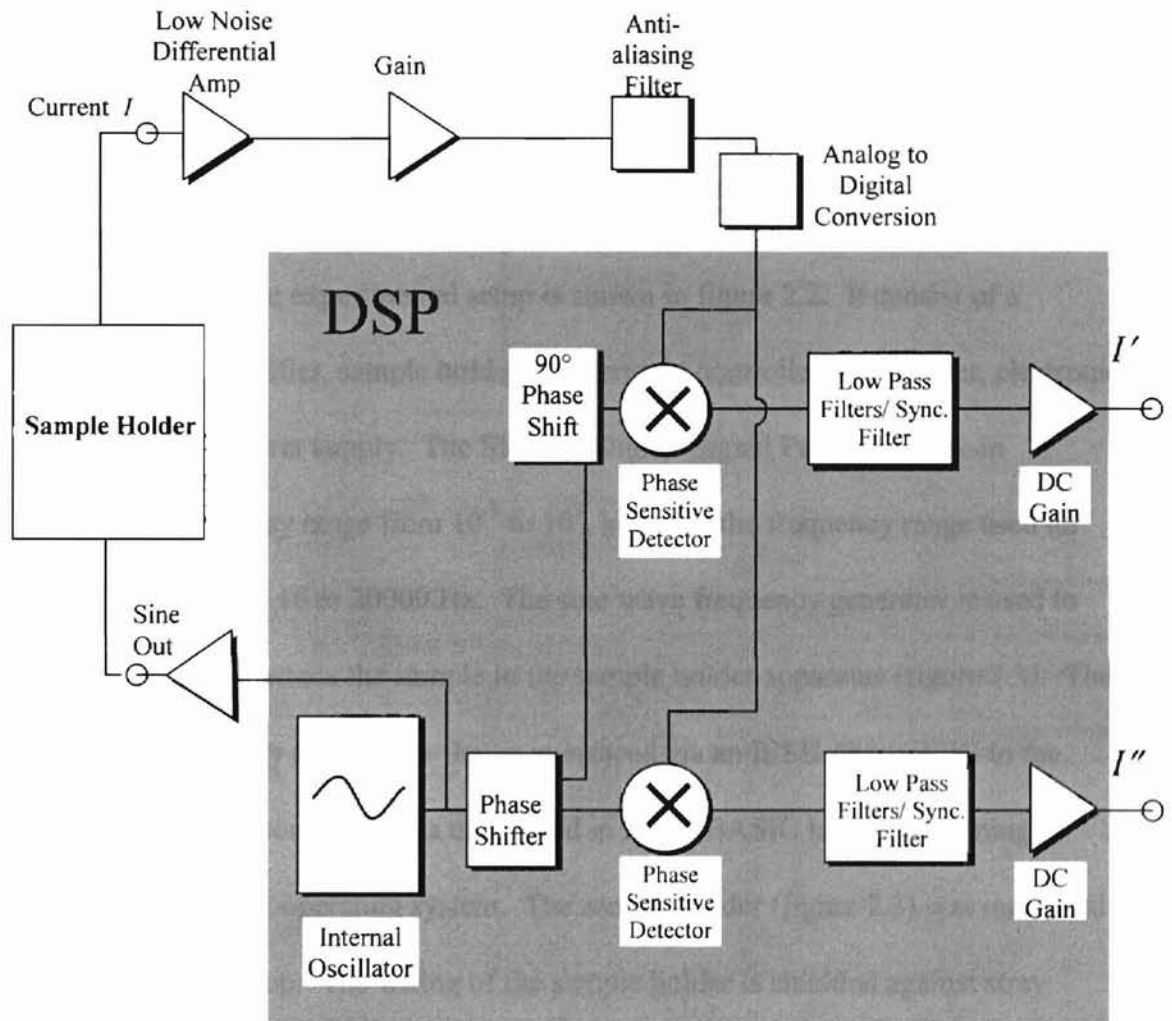
only the first term remains as the output:

$$V_o = (2/\pi) B \cos(\theta).$$

The output is a phase-sensitive dc voltage, with a maximum when $\theta = 0$. When the angular frequency of both input and reference are not equal ($\omega_r \neq \omega_i$), then the time average of the PSD output is zero, thus the PSD is frequency selective. As an exception to the above condition ($\omega_r \neq \omega_i$), the PSD output is non-zero if the input signal occurs in odd-order harmonics, i.e. $\omega_i = n \omega_r$, where $n = 3, 5, 7, \text{ and so forth}$ [16, 3]. Square-waves generate odd-order harmonics, as shown above. The PSD and low pass filter also removes noise from the experiment. The low pass filters allows only signals with frequencies close to the reference signal. Any other frequencies far above the reference signal are attenuated. Attenuation in this case depends on the bandwidth of the low pass filter. The narrower the bandwidth, the more noise removed close to the reference signal, but at the expense of possibly cutting off actual response signals. Wider bandwidth allows more noise to pass through as output [3]. With a lock-in, the frequency range is usually from 10^{-3} Hz to 10^5 Hz.

Figure 2.1 is a schematic of the Stanford Research SR830 DSP lock-in amplifier used in this study. Additional functions of the lock-in have been omitted since they were not used. The shaded area of figure 2.1 represents the lock-in components that have been integrated into a digital signal processor. A separate PSD multiplies with a 90° out of phase reference signal to derive the component that is out of phase from the original reference signal. A lock-in with two separate PSD is referred to as a dual-phase lock-in, such as the Stanford Research SRS830. One of the advantages of two PSDs is the ability of the lock-in amplifier to directly measure all of the components, real and imaginary, of

Figure 2.1 – SRS 830 DSP lock-in amplifier (after ref. 24)



the complex output signal. The internal digital reference signal generates a sine wave with a constant phase shift, which differs to the square wave generated by traditional analog lock-in amplifiers. As discussed above, square waves will result in odd order harmonics, which do not time average to zero. In this experiment, the internal reference signal is also used as the external signal, i.e. it is used to excite the sample. This is the reference [6, 3].

2.2 Experimental Setup

A diagram of the experimental setup is shown in figure 2.2. It consist of a computer, lock-in amplifier, sample holder, temperature controller, multimeter, electronic ice point, and a DC power supply. The SRS830 Digital Signal Processor lock-in amplifier has a frequency range from 10^{-3} to 10^5 , however the frequency range used on these glasses was from .16 to 20000 Hz. The sine wave frequency generator is used to generate an a.c. signal across the sample in the sample holder apparatus (figure 2.3). The SRS830 is automated by a computer that is interfaced via an IEEE-488 (GPIB) to the lock-in. The software controller was developed in HPIB-BASIC language running in Microsoft Windows 3.1 operating system. The sample holder (figure 2.3) was machined at the OSU machine shop. The wiring of the sample holder is shielded against stray capacitance by the use of coaxial cables. The inner chamber is well insulated to maintain a constant temperature and a constant pressure by allowing a slow leak. A type K thermocouple attached to an Omega MCJ ice point (chromel-alumel) is located an inch below the sample. The ice point is maintained at 1.35 volts by the use of a regulated DC power supply—the Lambda LQ-413. The internal thermocouple is attached to an

Figure 2.2 – Experimental setup

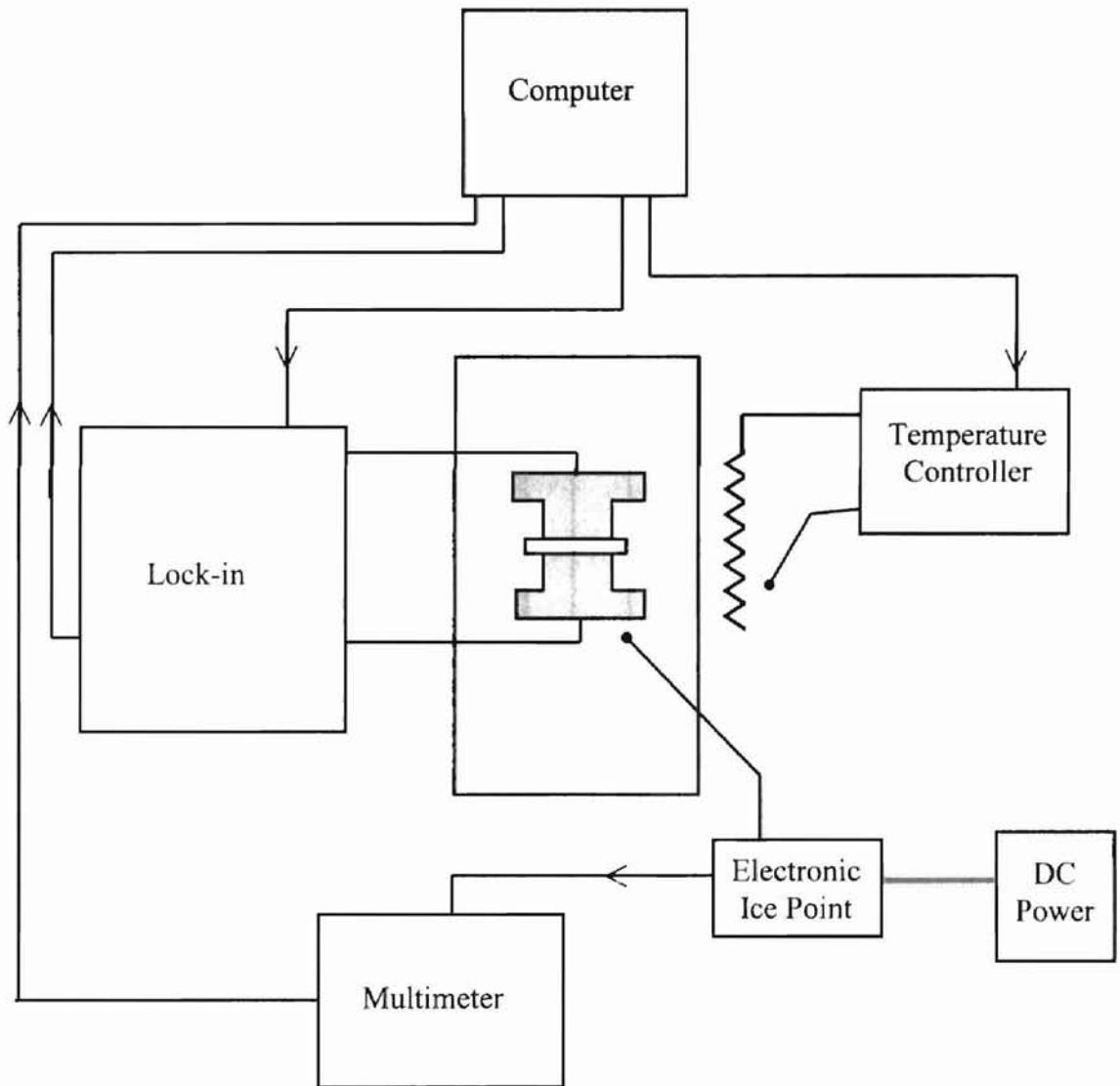
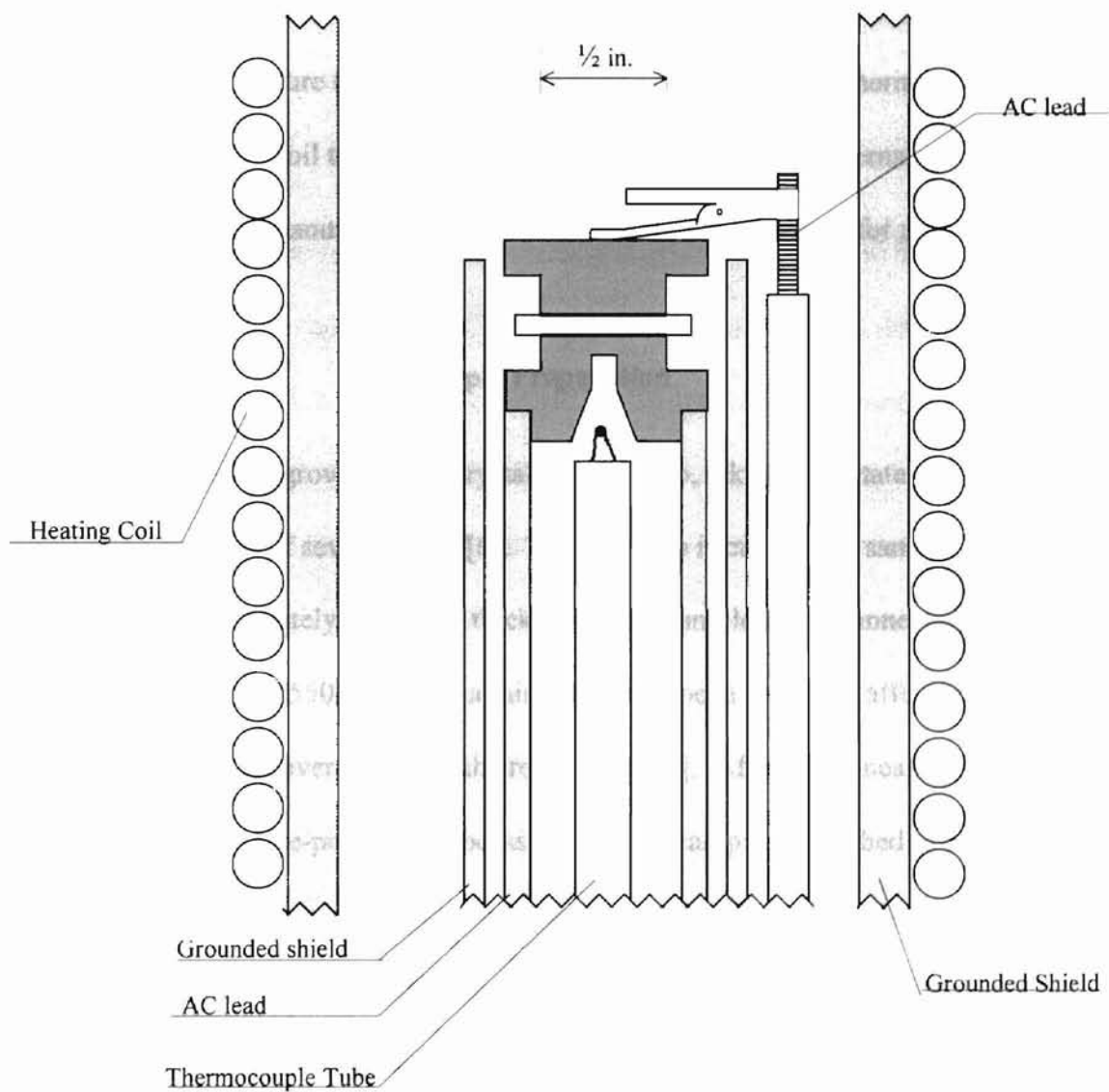


Figure 2.3 – Sample holder



HP 3478A multimeter. The HP3478A features a GPIB connector that is interfaced to the computer to automatically read the ambient temperature in the sample chamber. The temperature readings of the internal thermocouple fluctuated at about ± 0.001 mV that amounts to a $\pm 0.025^\circ$ fluctuations. An external heating coil is used to increase and maintain ambient temperature in the sample chamber. The heating coil is attached to the Omega CN-2000 temperature controller. For the temperature sensor, a thermocouple is attached near the heating coil to the CN-2000, which also features an internal ice point. The CN-2000 can be set manually but is also interfaced to the computer for automated setting of temperatures.

2.3 Sample Preparation

The samples were grown in the Crystal Growth Lab, Oklahoma State University. The preparation consists of several steps [6]. The first step is cutting the sample. Each sample is cut to approximately 0.5mm in thickness. The sample is then annealed for approximately 15 hours at 550 C. Thermal histories have been shown to affect the density of the sample and overall affects the resistivity [25]. After the annealing process, the sample undergoes a fine-polishing process. The glass sample is attached to a polishing holder using preheated rosin as the adhesion agent. The sample is then polished on a polishing wheel for approximately ten minutes on both sides. The polishing agent used is cerium oxide. Depending on the success of the cutting process, sometimes it's necessary to rough polish the sample at 600-grit. Once polished, the glass sample is soaked in acetone to remove all of the rosin. To ensure removal of ionic and metallic traces that may have built-up during the polishing process at the edges of the sample, the sample is also soaked in a hydrochloric and nitric acid solution for approximately 5

minutes. After the acid bath, the sample is rinsed with tap water and soap. Then the sample is ultrasonically cleaned in de-ionized water for 30 minutes. The final stage is to apply an Au-Pd plating over each sides of the sample. The plating is deposited using a Hummer V ion deposition chamber. Each side was exposed for 18 minutes to obtain good plating. A summary of the sample compositions along with the surface area dimension of the plating and thickness is listed in tables 2.0 and 2.1.

2.4 Experimental Procedure

To minimize surface conduction, the starting temperature is around 50°C [15]. Therefore, the temperature range between 50°C and 202°C is used in this study. The temperature coil was raised in 8°C increments, with a 1.5 hour wait between temperatures to reach equilibrium. The frequency of the internal sine wave generator is raised in 8% steps from .16 Hz to 20000 Hz. The SRS830 complex current output is transformed into its individual real and imaginary impedance components by using the relations derived from $V = I Z^*$:

$$Z'(\omega) = V_{rms} I'(\omega) / [I'^2(\omega) + I''^2(\omega)]$$

$$Z''(\omega) = V_{rms} I''(\omega) / [I'^2(\omega) + I''^2(\omega)]$$

where V_{rms} represents the rms amplitude of the reference sine wave. The Nyquist plots of sample Eu6 is shown in figure 2.4. The vertical straight line at lower frequencies in figure 2.4 is expected since the circuit model representing the sample and holder is an RC circuit in series with the double-layer capacitance. At lower temperatures, the low-frequency region of figure 2.4 does not quite intersect the real axis, which may be attributed to the double-layer capacitance. With increasing temperature, the plot gets closer to the real axis. The bulk resistance is determined by recording the value of the

Table 2.0 – Sample compositions

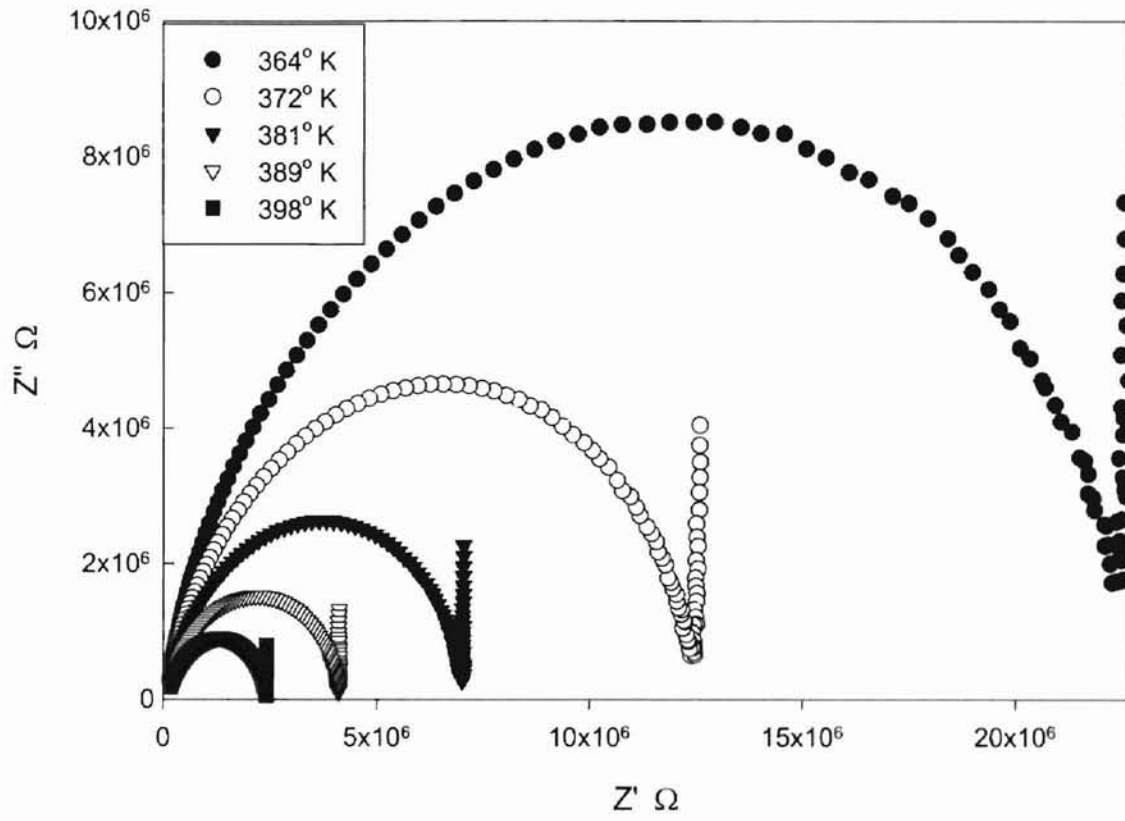
Component	Eu0	Eu6	Eu9	Eu12	Eu15	Na10	Na15	Na25
* SiO ₂	70	65.8	63.7	61.6	59.5	75	70	60
Al ₂ O ₃	3	2.82	2.73	2.64	2.55	3	3	3
MgO	12	11.28	10.92	10.56	10.2	12	12	12
Na ₂ O	15	14.1	13.65	13.20	12.75	10	15	25
Eu ₂ O ₃	0	6	9	12	15	2.5	2.5	2.5

* Base composition

Table 2.1 – Sample dimensions

Sample	Thickness (cm)	Area (cm ²)	$I/A (\pm 3\%) \text{ cm}^{-1}$
Eu0	0.0534	1.75	0.0305
Eu6	0.0550	0.907	0.0606
Eu9	0.0473	0.630	0.0751
Eu12	0.0548	0.467	0.117
Eu15	0.0568	0.403	0.141
Na10	0.0577	1.600	0.0361
Na15	0.0490	0.790	0.0620
Na25	0.110	0.630	0.175

Figure 2.4 - Nyquist Plot of 6% Europium



real axis at the point in which the Nyquist plot is least imaginary (or comes closest to the real axis). The conductivity is determined using the relation $\sigma = d/(A Z')$, where d is the sample thickness, A is the plating area, and Z' is the real impedance. The conductivity is calculated at each temperature step and then fitted to an exponential decay curve, $y = a \exp(-b x)$. The known parameters are $x = 1/(k_b T)$, and $y = \sigma T$. Using Microsoft Excel for an exponential fitting, the parameters b (activation energy in this case), and the pre-exponential factor, a , are determined. The frequency dependent characteristics can be determined directly from the impedance data by using the equations as summarized at the end of chapter 1.

CHAPTER III

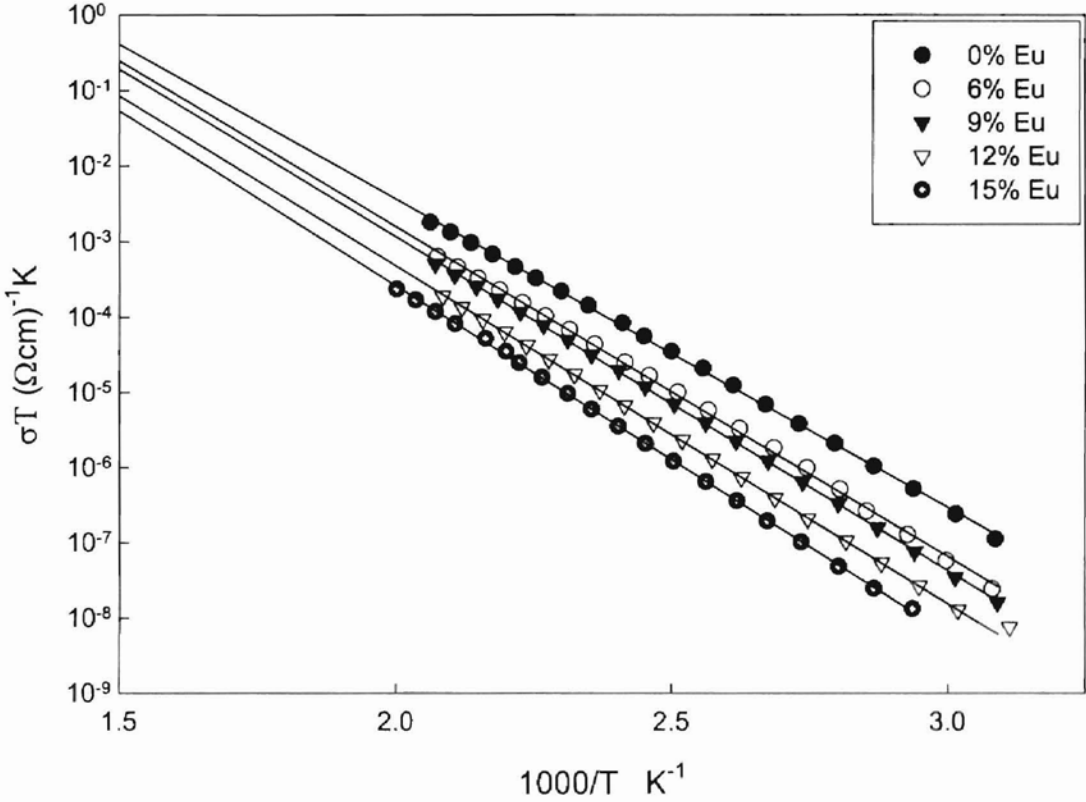
RESULTS AND DISCUSSION

3.1 Activation Energy and Conductivity

The conductivity of the europium and sodium series of samples is of particular interest to investigate further the results of LIG experiments. This experiment showed a decrease in conductivity of the europium set as a function of increasing europium concentration. Many published experiments have established that $(\text{Na}_2\text{O})_x (\text{SiO}_2)_{1-x}$ type glasses have shown an increase in conductivity with increasing sodium concentration. Likewise, this experiment showed an increase of conductivity in the sodium series with increasing sodium concentration. Previous experiments [6] on glasses in the family studied here have also shown an increase in conductivity with the increase of Al_2O_3 , however LIG experiments in this case had opposite results for both samples. In LIG experiments (A.Y. Hamad private communication), the sodium series showed a decrease in grating formation efficiency, however, the aluminum series showed an increase in LIG grating formation. In the case of the europium series, the LIG results showed an increase in efficiency. The main interest is to investigate the conductivity measurements in hopes of further investigating the decrease in efficiency in four-wave mixing.

Arrhenius plots of the europium series is shown in figure 3.1. A shift to the left with increasing Eu^{3+} concentration indicates a decrease in conductivity. To effectively show this decrease, the conductivity as a function of europium concentration at temperatures of $81 \pm 2^\circ\text{C}$ and $104 \pm 2^\circ\text{C}$ centigrade is extracted from figure 3.1 and shown

Figure 3.1: σT Vs. $1000/T$ of Europium Series



in figure 3.2. The plot in figure 3.2 also shows that the conductivity is increasing as a function of temperature from 81°C to 104°C. There appears to be a larger gap between decreasing conductivities from the base glass samples to the samples with europium content. This wider gap can be attributed to the base sample having a contribution from both NBO bound mobile ions, and aluminum tetrahedra bound sodium ions. Since there are no europium ions that can reduce the conductivity of the base sample, the base sample is more conductive. The samples with europium content of 6% to 15% exhibited slight shifts to the left, which indicates a slight decrease in conductivity. This is in agreement with studies done on P_2O_5 base glass with praseodymium dopants, which have also shown a decrease in conductivity [26]. Figure 3.3 shows the activation energy as a function of increasing Eu^{3+} concentration. The activation energy is extracted by using an exponential fit of the Arrhenius plot from Figure 3.1. The increase in activation energy (figure 3.3) follows the decrease in conductivity (figure 3.2). Table 3.1 lists the activation energy and exponential pre-factor in table 3.2 for both families of samples.

The decrease in conductivity is a consequence of the glass structure that results from the addition of the Eu_2O_3 glass modifier. One obvious reason is that an increase of Eu_2O_3 inherently decreases the Na_2O concentration, thus decreasing the availability of mobile ions. Another reason can be seen from figure 1.3. The introduction of europium oxides results in the formation of three types of NBO's in the glass structure, i.e., Q_1 , Q_2 , and Q_3 species can exist [7]. The NBO's are charge compensated by Sodium (Q_3 Species), and Europium ions (Q_2 , and Q_1 Species). One speculation is the ionic radius of europium is comparable to the inter-atomic distance between the Si-O that can result in the Eu^{3+} being intertwined within the glass structure such that it does not locally charge

Table 3.1 – Activation energy of Eu and Na samples

Sample	E_a (eV)
Eu0	0.813
Eu6	0.871
Eu9	0.880
Eu12	0.892
Eu15	0.918
Na10	0.830
Na15	0.832
Na25	0.793

Table 3.2 – Exponential Pre-factor of Eu and Na samples

Sample	σ_0 (ΩCm) ⁻¹
Eu0	575803
Eu6	950128
Eu9	872564
Eu12	468483
Eu15	472655
Na10	513000
Na15	708000
Na25	929000

Figure 3.2: Conductivity Vs Europium Concentration

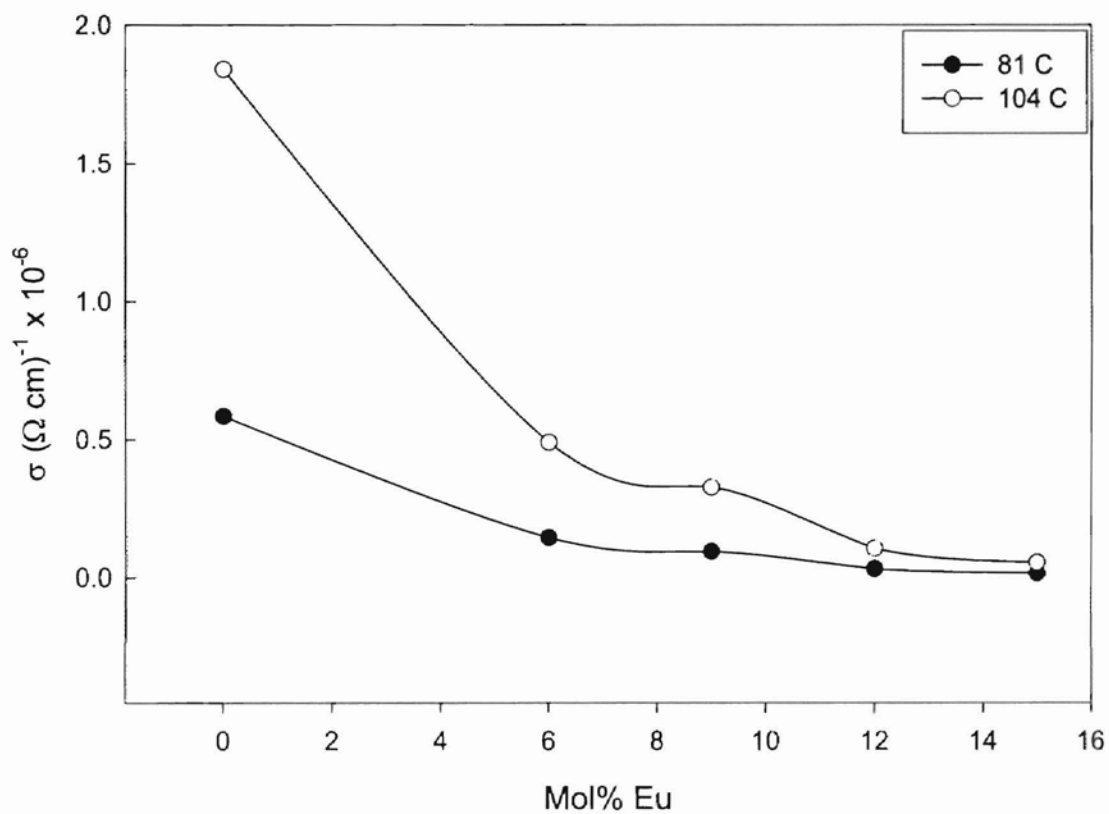
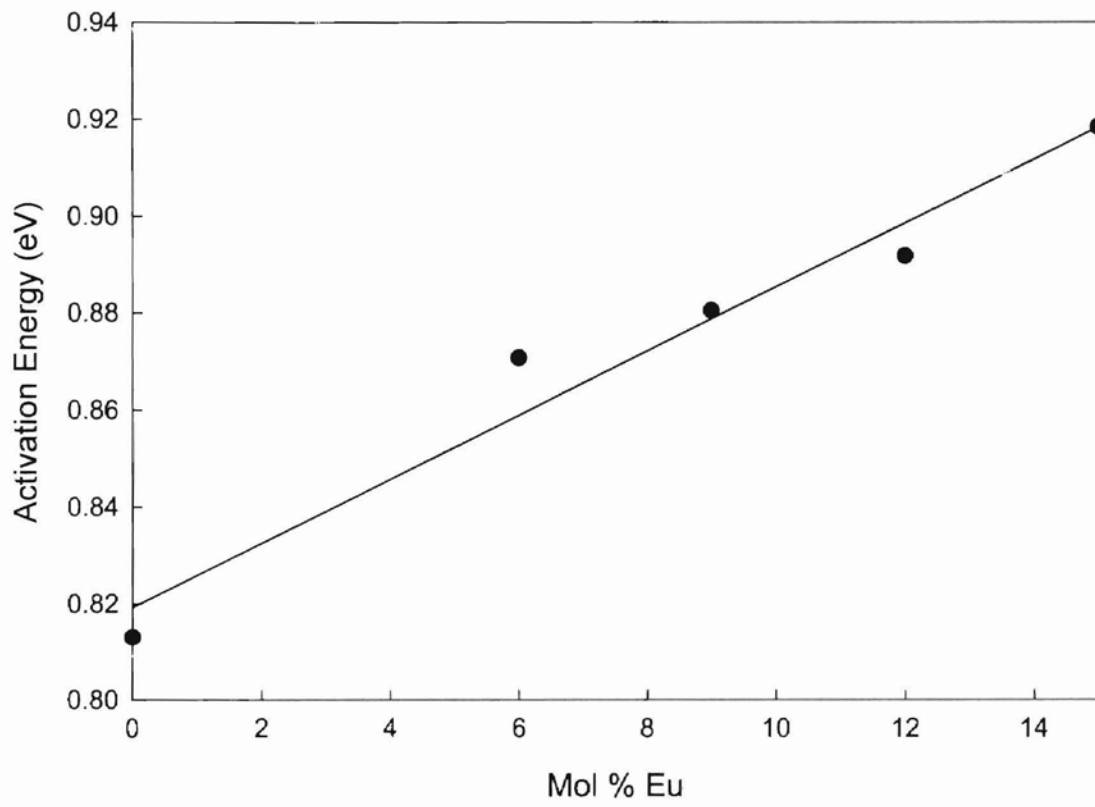


Figure 3.3: Activation Energy Vs Mol% Eu



compensate any of the NBO's. The NBOs, which are not locally charge compensated, act as holes that traps mobile modifiers, thus increasing the average activation or binding energy [G.S. Dixon private communication]. It is further noted that x-ray-absorption fine structure experiments (XAFS) spectroscopy, and computer simulation shows evidence that network modifiers, i.e. alkali, alkaline-earth, rare-earths, tend to cluster along the percolation pathways of migrating ions [24]. Therefore, its possible that europium ions can occupy NBO sites close to those of sodium ions, that can cause a blocking effect due to the ionic radius of the europium. Hence, increasing the concentration of the Eu_2O_3 modifier decreases the mobility of Na^+ ions.

Figure 3.4 is the Arrhenius plot of the sodium series. As expected, the graph with increasing concentration of sodium ions is shifting to the right, which follows an increase in conductivity (figure 3.5). The 10% and 15% samples nearly overlap. Figure 3.5 shows the trend of the conductivity with increasing concentration of sodium. As before, the conductivity is also higher with increasing temperature. The average activation energy is shown in figure 3.6. The trend of the activation energy is decreasing, which follows the increasing conductivity. The difference in activation energy between the 10% and 15% sample is minimal, which is due to the "overlap" seen in figure 3.4. From various studies, it is established that that sodium ions are the primary charge carriers in these family of samples [4, 11,12,14,15]. Computer simulation studies have shown that alkali ions migrate along the interstices formed by the NBO's [8, 24]. As discussed above, XAFS gives evidence of clustering in alkali ions along the interstices pathways. Therefore, as the Na concentration increases, one expects the sites of lowest energy (deepest wells) to fill first, thus higher Na concentration samples have lower average

Figure 3.4 - σT Vs. $1000/T$ of Sodium Series

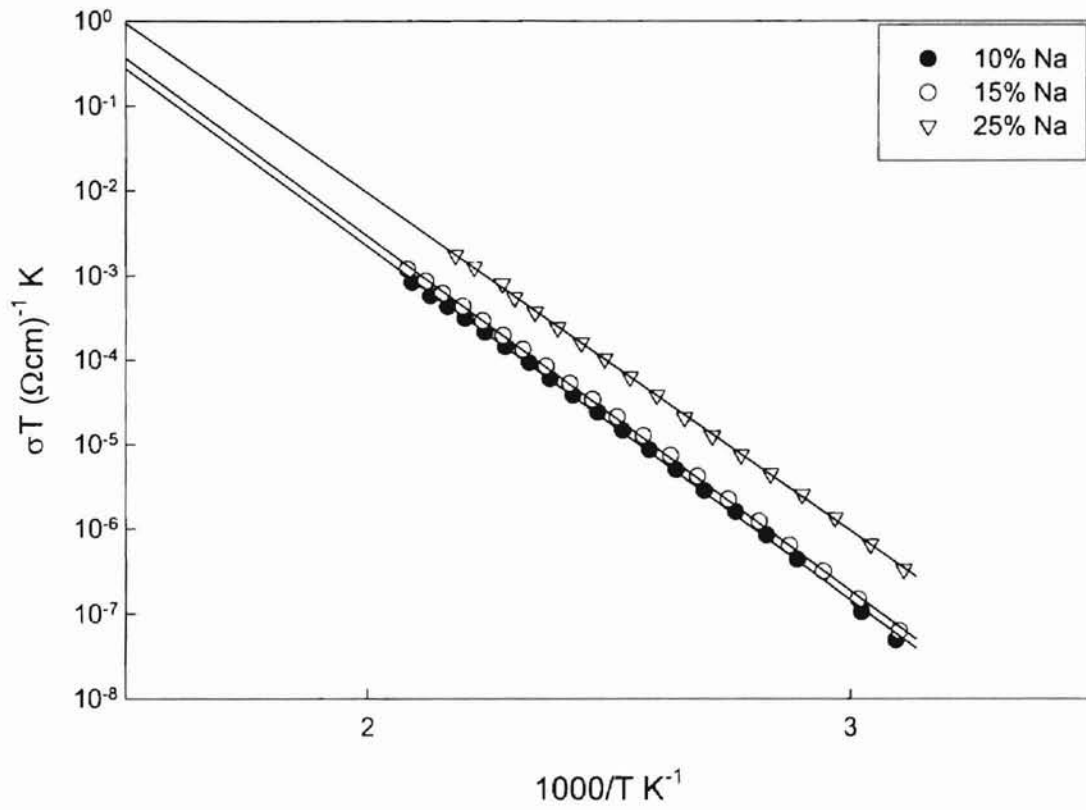


Figure 3.5: Conductivity Vs Sodium concentration

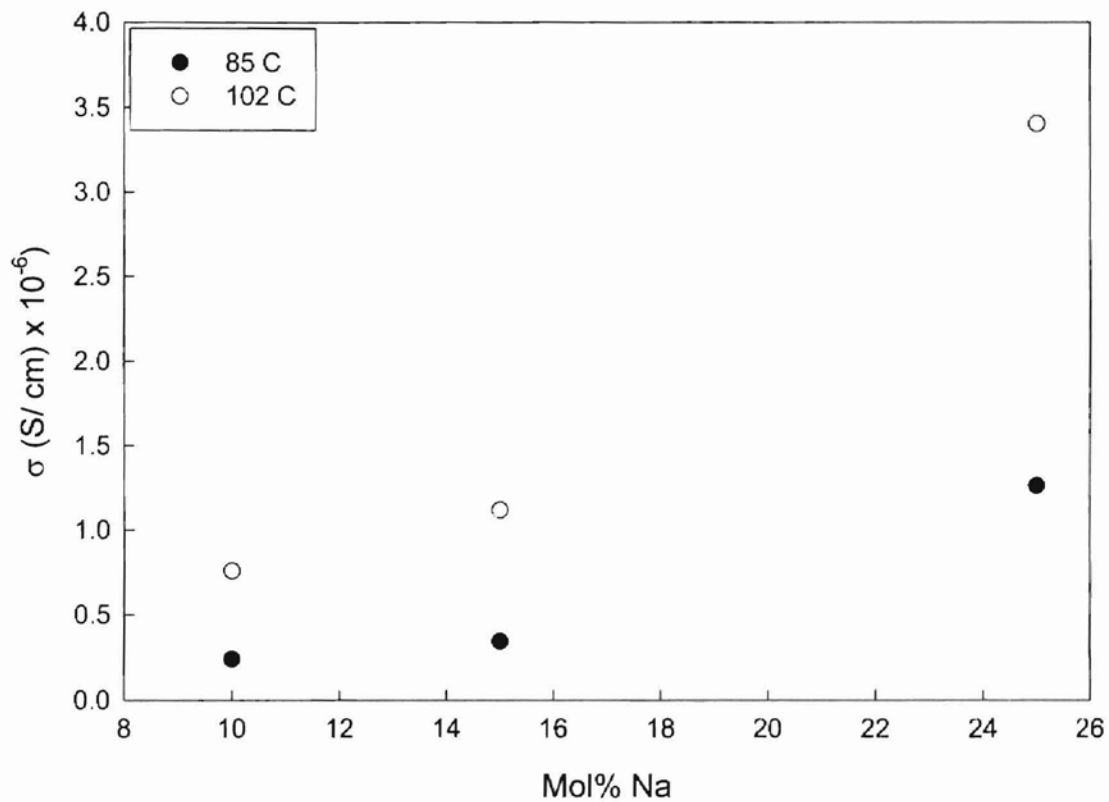
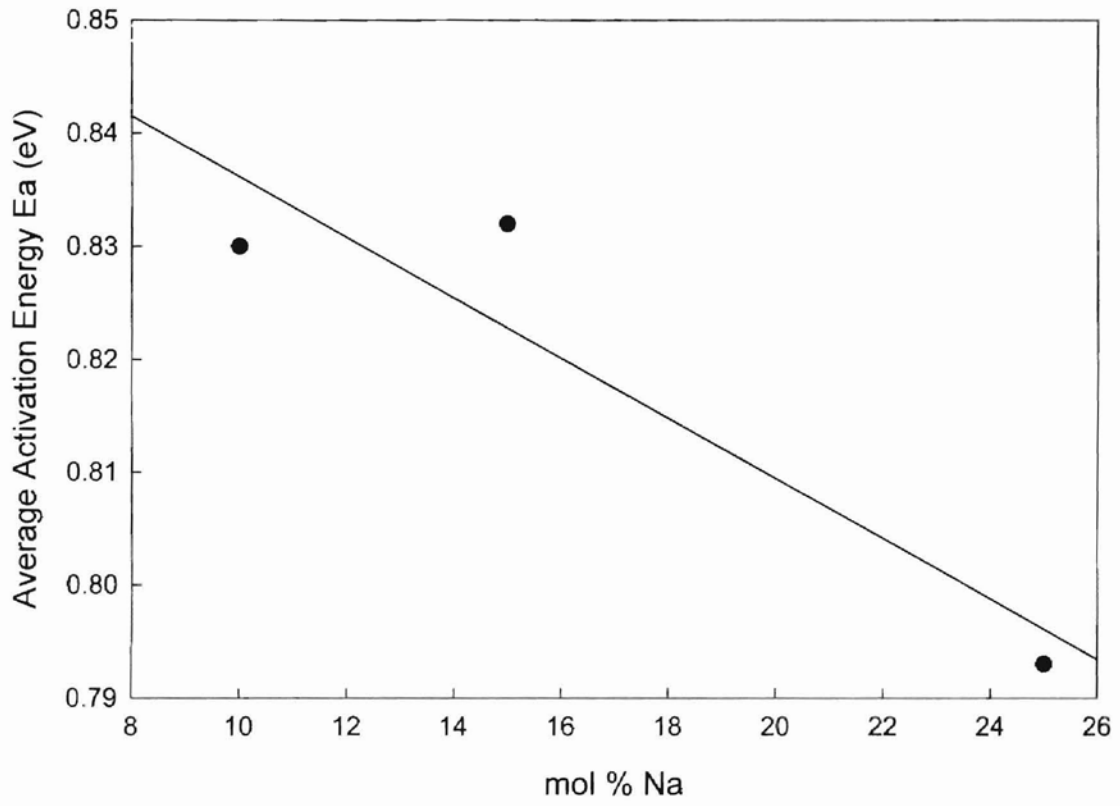


Figure 3.6 - Activation Energy E_A Vs. Mol % Sodium



activation energies due to the greater fraction of Na in shallow sites [Dr. G.S. Dixon private communication].

The pre-exponential factors shown in table 3.2 are highly dependent on the temperature range on which the conductivity measurements are made; hence, assigning any significance to the data may be spurious. The data does have a trend in conjunction with the type of sample. For samples Eu6 to Eu15, the pre-exponential factor decreases as a function of increasing europium concentration, with the exception of Eu0, which lacks europium dopants. As a final note, the activation energy of Eu0 (table 3.1) is in range between the Na15 and Na25 samples. In fact, the conductivity of Eu0 is greater than sample Na15. This is not surprising since Na15 contains a 2.5% europium dopant, while Eu0 has none; therefore, Eu0 should have a greater conductivity and lower activation energy as compared to Na15.

3.2 Dielectric Analysis

A plot of M' vs. f is shown in figures 3.7.a and 3.7.b. The data is obtained from the 25% Na sample and 12% Eu sample, respectively. Successive temperature ranges from 321K to 368K shows the modulus converges to zero at low frequencies. This suggests a negligible contribution to the electrode-material layer capacitance; therefore, it can be ignored when data is analyzed in the modulus formalism [9]. At higher frequencies, it appears to be converging to a constant value. The imaginary component as a function of frequency ($M'' = \omega C_o Z'$) is shown in figure 3.7.c for the Europium series at $104 \pm 2^\circ$ C. The plot is normalized to peak, M''/M''_{peak} . It is immediately apparent

Figure 3.7.a - M' vs. frequency of 25% Na

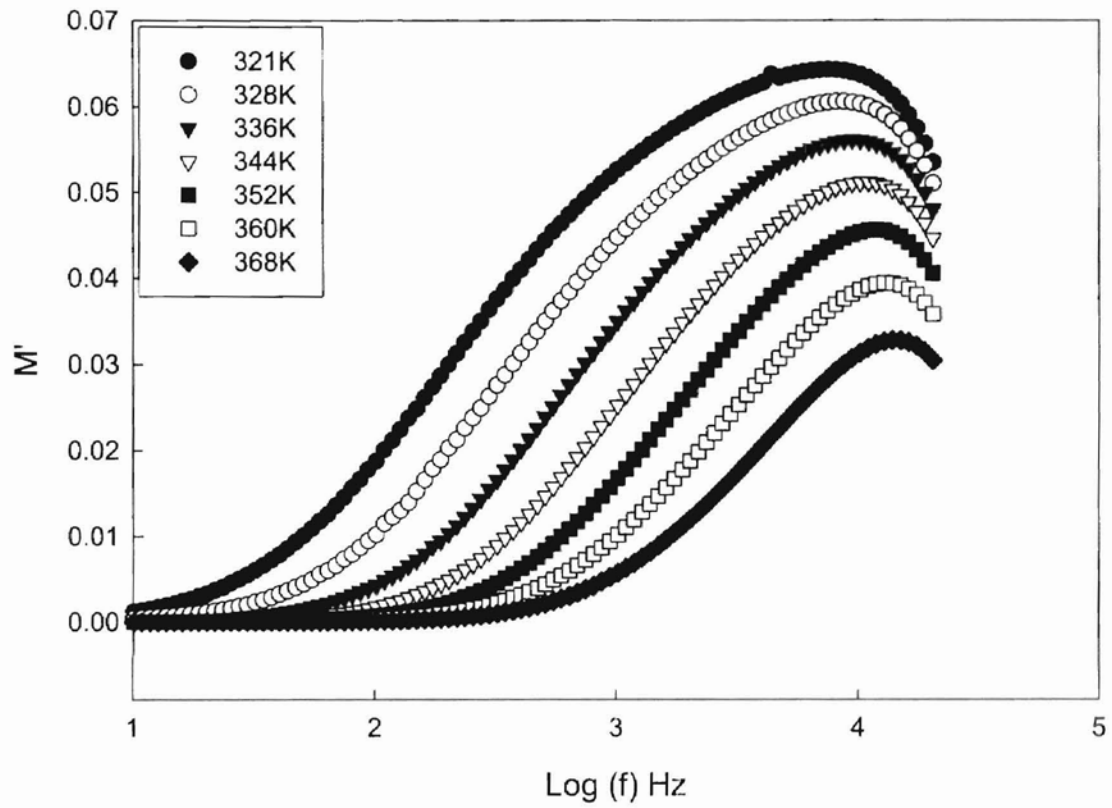
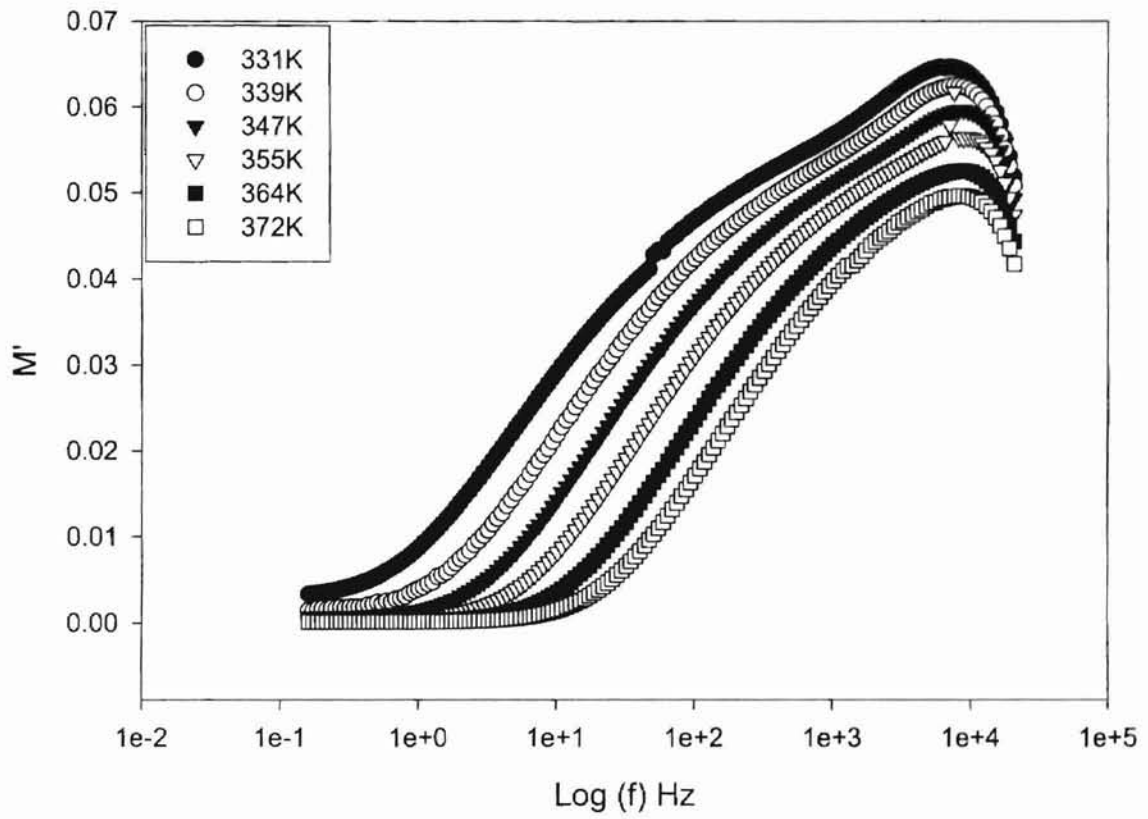


Figure 3.7.b - M' vs. frequency of 12% Eu



that the peaks are much broader compared to the ideal Debye peak of 1.14 decades FWHM. The broad peak indicates a distribution of relaxation times, as expected from Stevels model of random barriers. The relaxation time of long-range migration can be calculated by using the peak frequency, $\tau = 1/\omega_{peak}$, of M''/M''_{peak} . With the apparent decrease in conductivity as europium concentration, one would expect the relaxation time to increase with increasing europium concentration. The region to the left of the peak is the region in which a significant amount of migration involving long distances (long-range conductivity) can occur, whereas the region to the right involves mostly the migration of ions over short-distances. The plot in figure 3.7.d exhibits the same type of peaks as in figure 3.7.c, but with opposite shifts as a function of concentration. The shifts to the right (figure 3.7.d) are expected for the sodium series with increasing conductivity.

Figure 3.8.a shows the plot of the frequency dependent dielectric constant for the samples Eu0 to Eu15. The plot is broken down into two regions at the low frequency, and high frequency. At low frequencies, the dielectric constant is decreasing as a function of increasing europium concentration. Since ionic migration dominates the dielectric constant at low frequencies, the trend of the dielectric constant follows the d.c. conductivity which is already established to decrease as a function of europium concentration. As the frequency is increased, the dielectric constant for the europium set crisscrosses. At higher frequencies, instant polarization or electronic polarization dominates. Likewise, the dielectric plot of the sodium set Na10 to Na15 is shown in figure 3.8.b. Again, there are two regions of interest. At low frequency, the dielectric is increasing as a function of sodium concentration. This time, ionic migration increases as a function of sodium concentration, therefore, an increase in dielectric with respect to

Figure 3.7.c - M''/M''_{peak} vs. Frequency at 104°C

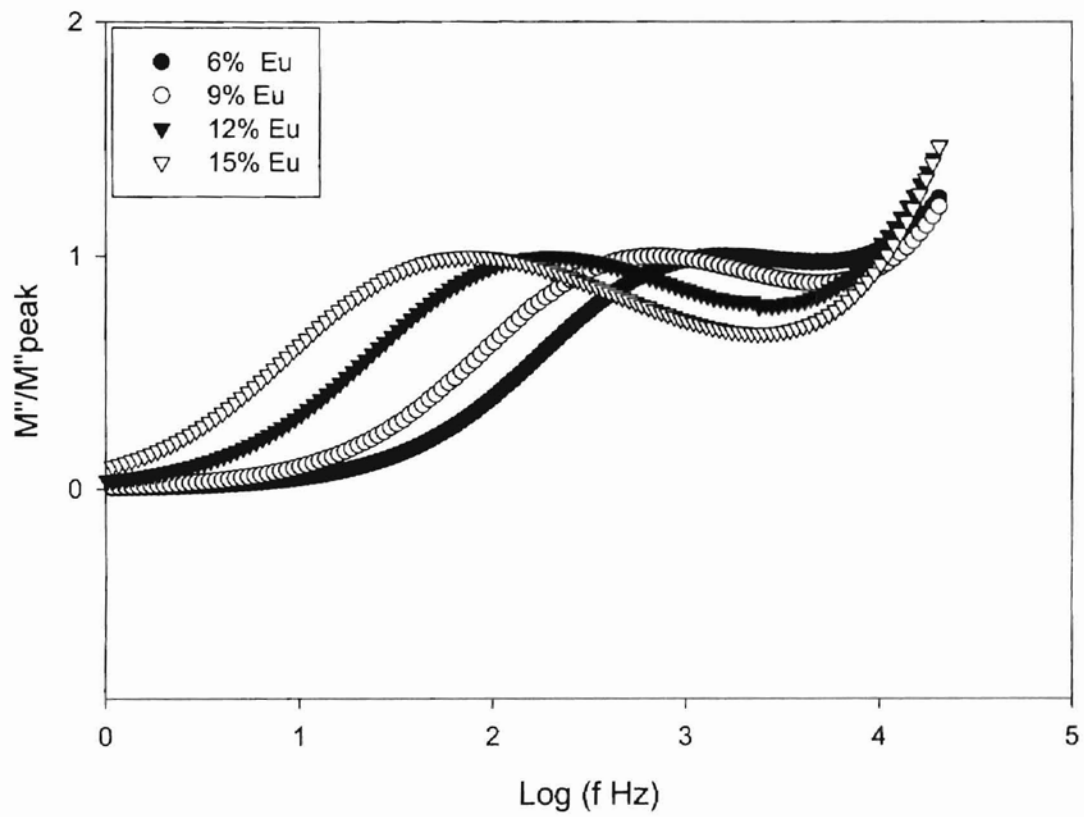


Figure 3.7.d - M''/M''_{peak} vs. frequency at 104°C

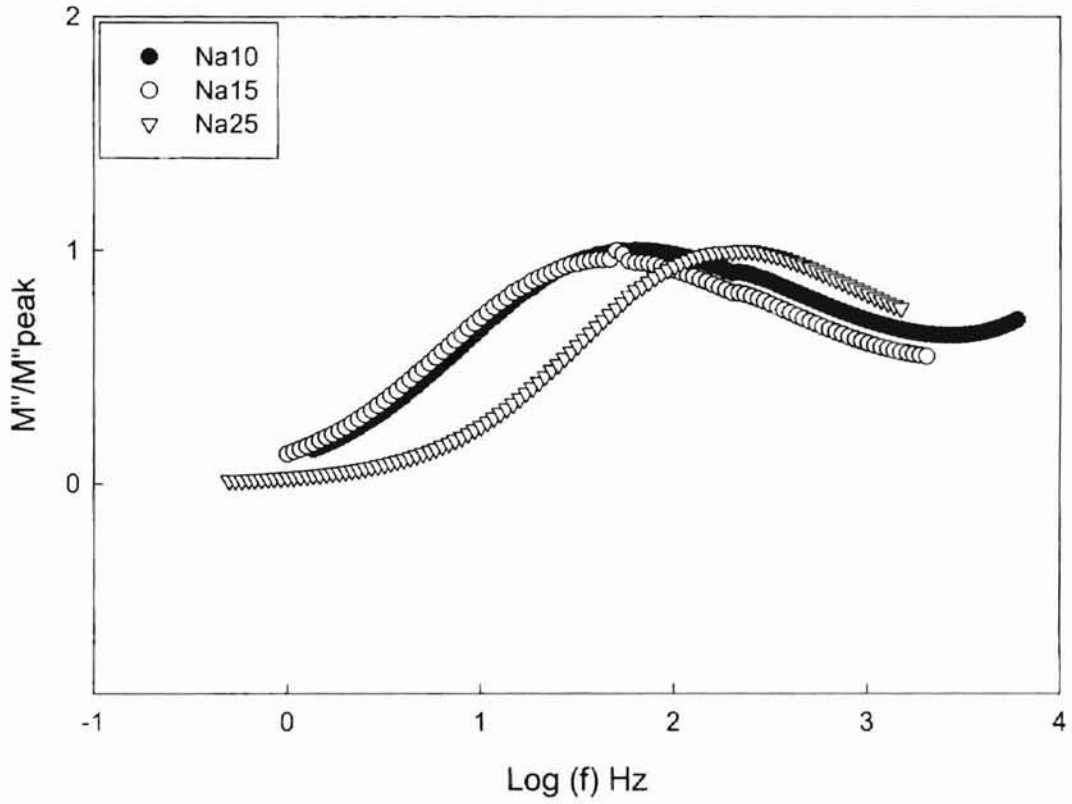


Figure 3.8.a - Dielectric constant vs. Frequency at 102°C

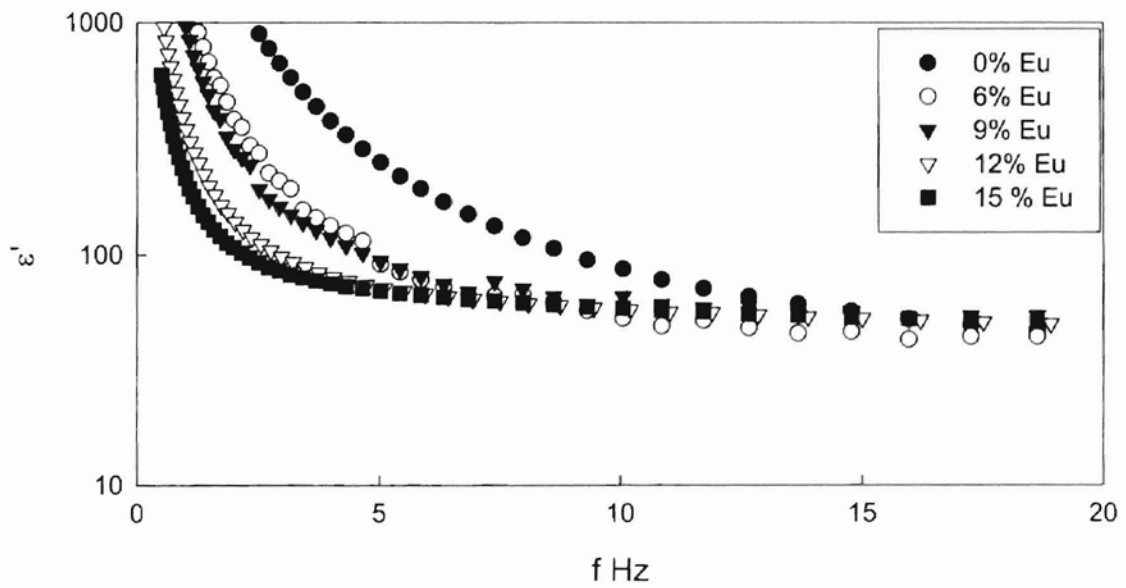
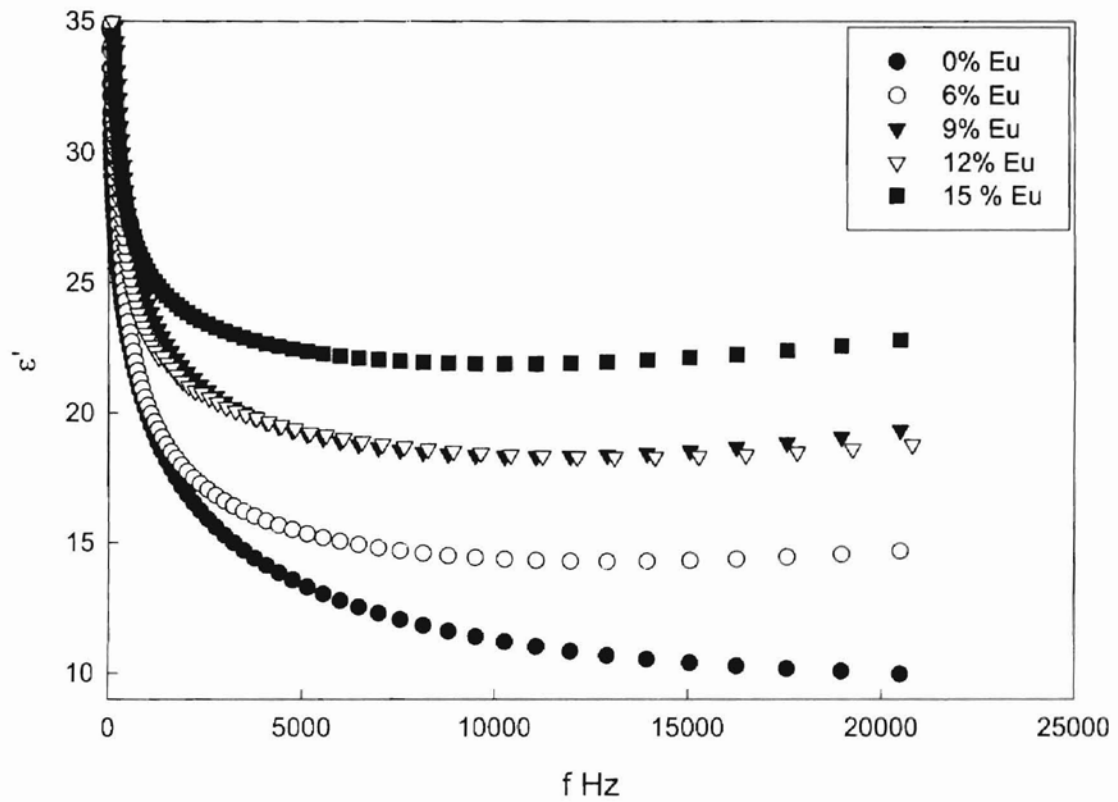
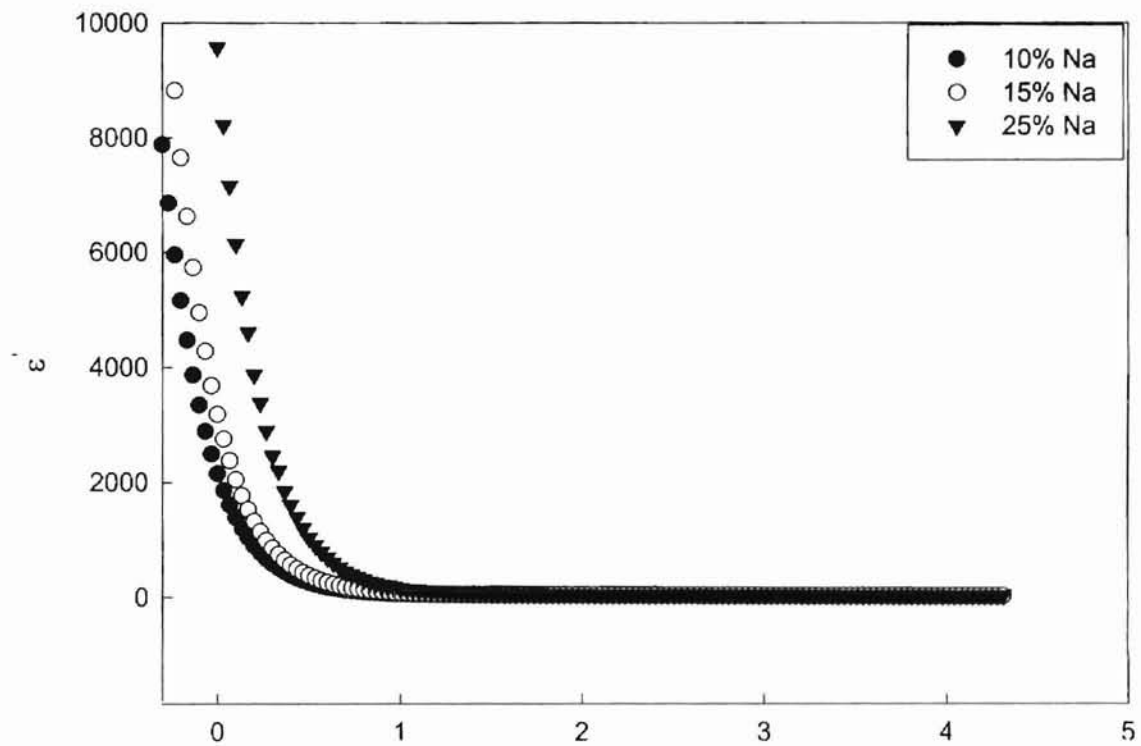


Figure 3.8.b - Dielectric constant vs. Frequency at 100°C



increasing sodium is expected. At higher frequencies, the dielectric function converges and seems to flatten out. The dielectric data is still increasing as a function of sodium concentration meaning there's a minimal contribution to electronic polarization.

The log-log plot of the loss angle vs. frequency for the europium series at 104°C is shown in figure 3.9.a. At the lower frequencies, the losses reach a maximum that corresponds directly to the frequencies where the sample becomes purely resistive. The shift to the left as a function of increasing europium concentration indicates a decrease in the losses. This is expected due to the decreasing conductivity with respect to increasing europium concentration. The less mobile the ions, the less energy are lost into the glass network. At higher frequencies, the loss appears to increase and converge. In contrast, the plot in figure 3.9.b shows the loss angle vs. frequency of the sodium series. The low frequency and high frequency features are similar to the europium series. However, the plot shifts to the right as a function of concentration, which follows the increase in conductivity.

3.3 Conclusions on Laser Induced Experiments

LIG experiments in glasses as a function of increasing europium have shown an increase in grating formation efficiency [A.Y. Hamad private communication]. It is believed that the migration of energetic ions, driven by the nonradiative relaxation of europium, is responsible for the grating formation. The europium series studied in this thesis showed an increase in activation energy as a function of increasing europium concentration. This increase in activation energy suggests a decrease in grating formation. However, that is not the case from LIG experiments since grating formation

Figure 3.9.a - Loss Angle vs Frequency for Europium Series at 104°C

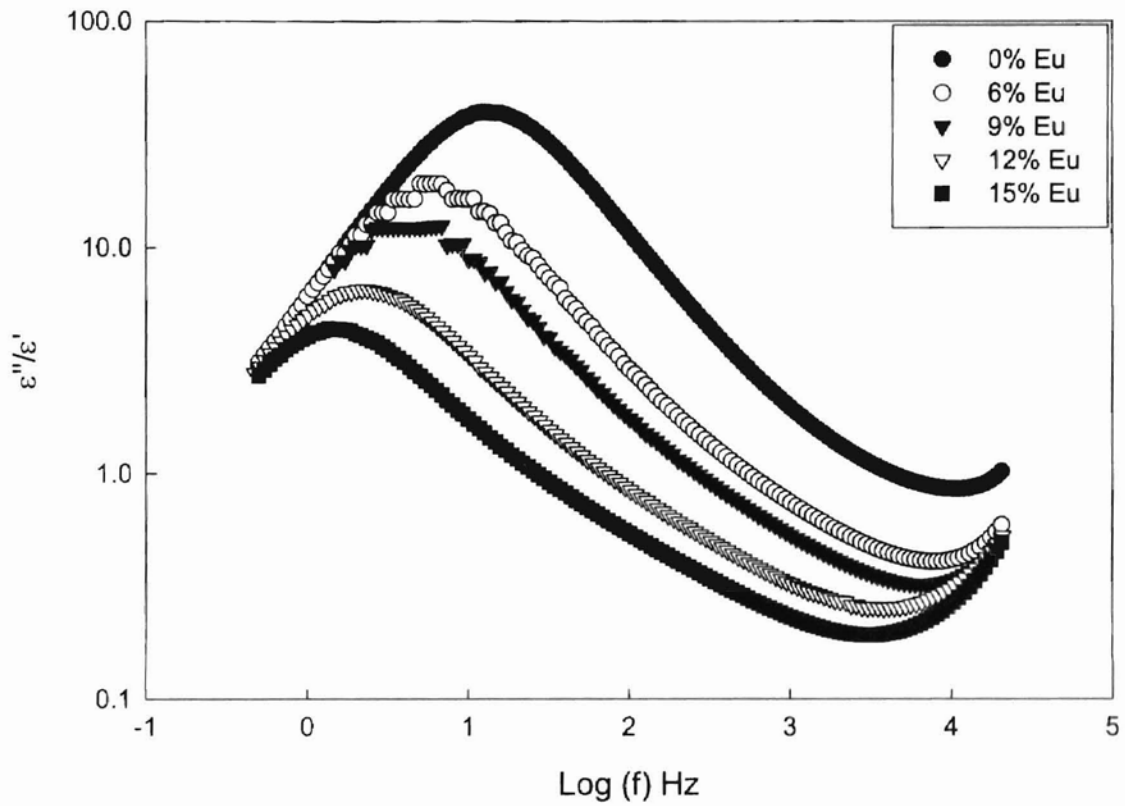
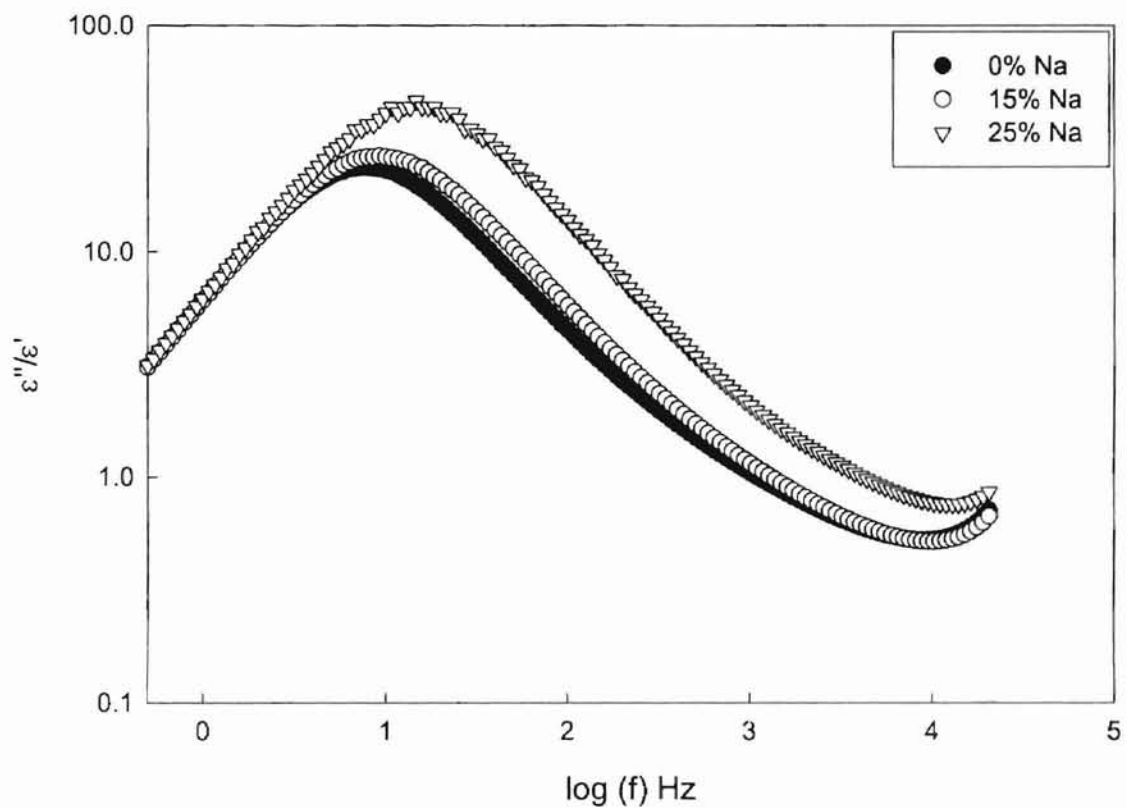


Figure 3.9.b - Loss Angle vs Frequency for Sodium Series at 104°C



efficiency did increase. A possible explanation to the increasing LIG efficiency is that the ionic migration involves a localized ion migration, thus mostly short-range movements within the interstices of the glass. The activation energy gained from impedance spectroscopy represents the d.c. bulk conductivity. Another explanation is that the nonradiative relaxation of europium may have enough phonon energy to readily cause magnesium ions to migrate, in addition to the sodium ions, whereas magnesium is not readily mobile in ionic conductivity studies.

In the sodium series of glasses, LIG experiments showed a decrease in efficiency as sodium oxide is increased [A.Y. Hamad private communication]. The Eu^{3+} content in these glasses were kept constant at the expense of other components (see table 2.0). From XAFS and computer simulations, the evidence of sodium clustering may decrease the grating efficiency since there may not be enough europium for phonon excitation of the migrating ions.

CHAPTER IV

CONCLUSION

In this study the thermally activated d.c. conductivity and frequency dependence of aluminosilica glass have been measured. The composition of the aluminosilica glasses consisted of $1-Y (Na_2O \ 12MgO \ 3Al_2O_3 \ 70SiO_2) \ YEu_2O_3$ and $1-X(12MgO \ 3Al_2O_3 \ 70SiO_2) \ XNa_2O \ 2.5Eu$, where $Y = 0, 6, 9, 12, 15$ and $X = 10, 15, 25$.

It was shown that the dc conductivity data is Arrhenius-like in behavior. The activation energies were derived by the fitting of the Arrhenius plots. In the europium series, the activation energy increased with increasing europium content. This increase has been attributed to the clustering of europium ions as a function of increasing concentration. The clustering of europium has the effect of blocking the mobile ions.

On the other hand, the dc conductivity data of the sodium series was opposite to the europium series. As expected, the activation energy of the sodium set decreased as a function of increasing Na concentration. The increase of Na concentration readily provided excess sodium ions that are well established as the primary mobile ion.

In the modulus analysis, the relaxation times increased as a function of increasing Eu concentration. This follows the increasing activation energy, since the relaxation time represents the average time in which an ion will “hop” over an energy barrier. Likewise, the relaxation times decreased as a function of increasing Na, which follows the decreasing activation energy as a function of increasing Na concentration.

The dielectric function dependence of the europium set showed two different regions of interest in the frequency. At low frequency, the dielectric constant decreased as a function of increasing europium concentration. This is attributed to the decreasing conductivity as Eu concentration is increased. At higher frequencies, the increase in the dielectric constant as a function of Eu concentration suggests electronic polarization is more dominant, as expected due to the vastly different electron configuration the europium ion has compared to the other compositions in the glass structure. In comparison, the sodium at low frequencies exhibited a vast increase in the dielectric function as Na concentration is increased. This is attributed to the increasing long-range mobility associated with an increase of sodium ions. At higher frequencies, the dielectric function converged to a lower value regardless of Na concentration. However, the dielectric data still showed slight increase as a function of Na concentration.

In comparison to four-wave mixing, there was no direct correlation to ionic conductivity studies. Four-wave mixing experiments involve a different process in ion hopping as compared to ionic conductivity studies. In ionic conductivity studies, the external temperature provided the thermal excitation of mobile ions. Likewise, in four-wave mixing experiments, the nonradiative relaxation of europium is the primary thermal source in ion hopping. Furthermore, it is also speculated that ion hopping in LIG experiments may involve short-range migration [A.Y. Hamad private communication], rather than long-range migration which is more dominant in ionic conductivity studies at low frequencies. In conclusion, the opposite results between four-wave mixing experiments and ionic conductivity experiments are expected.

REFERENCES

- [1] Glass Science by Doremus, Robert H. (John Wiley & Sons, New York, 1994).
- [2] Glass Science and Technology: Glass-Forming Systems Vol.1 edited by Uhlmann, D.R., and Kreidl, N.J. (Academic Press, New York, 1983).
- [3] Model SR830 DSP Lock-In Amplifier Technical Manual (Stanford Research Systems, Inc., Sunnyvale, 1993).
- [4] Dynamics of Na in sodium aluminosilicate glasses and liquids, George, A. M., Stebbins, J. F., Physical Chemistry Minerals (1996) vol. 23 pp 526-534.
- [5] Materials Science and Technology: A Comprehensive Treatment Vol. 9, edited by Cahn, R.W., Haasen, P., Kramer, and E.J.
- [6] Mike Hogsed, MS Thesis, Oklahoma State University (1999).
- [7] Zhandos Utegulov, MS Thesis, Oklahoma State University (1999).
- [8] Dc and Ac Conductivity in Wide Composition Range Li₂O-P₂O₅ glasses, Martin S.W., Angell C.A., Journal of Non-Crystalline Solids 83 (1986) 185-207.
- [9] Gargouri, M. Solids State Ionics 100 (1997) 225-232.
- [10] Physics of Solid Dielectrics by Ion Bunget, Mihai Popescu(Elsevier, New York, 1984)
- [11] Introduction to Glass Science And Technology, James E. Shelby (The Royal Society for Chemistry, Cambridge, UK, 1997).
- [12] Solid State Chemistry and It's Applications, Anthony R. West (John Wiley & Sons, new York, 1984).
- [13] Progress in Ceramic Science vol. 3, edited by J.E. Burke (The Macmillan Company, New York, 1963).
- [14] Properties and Applications of Glass, Glass Scinece and Technology 3, H. Rawson (Elsevier Scientific publishing Company, NY, 1980).

- [15] J.M. Stevels, Encyclopedia of Physics, Vol. 20, 350 (Springer Verlag, Berlin, 1957).
- [16] Impedance Spectroscopy, edited by J. Ross McDonald (John Wiley and Sons, New York, 1987).
- [17] Dielectric Materials and Applications, edited by Arthur von Hippel (Artech House, Boston, London, 1995).
- [18] Electrode Kinetics, Eliezer Gileadi (VCH Publishers, Inc., New York, 1993).
- [19] J.C. Dyre, Journal of applied Physics, 64, 2468 (1988).
- [20] Dielectrics, by J.C. Anderson (Reinhold Publishing Corporation, New York, 1964).
- [21] B.V.R. Chowdari, R. Gopalakrishnan, Solid State Ionics, 23, (1987), 225-233.
- [22] Electric Circuits, James W. Nilsson (Addison-Wesley Publishing Company, 1994).
- [23] An Introduction to Electrical Instrumentation and Measurement Systems, B.A. Gregory (John Wiley and Sons, New York, 1981).
- [24] G.N. Greaves, K.L. Ngai, Physical Review B, Vol 52, Number 9, (1995).
- [25] Electrical Conductivity in Ceramics and Glass, edited by Tallan, Norman M. (Marcel Dekker, New York, 1974).
- [26] C.A. Hogarth, M.N. Khan, Journal of Non-Crystalline Solids, 123, (1990), 339-343.
- [27] Abdulatif Y. Hamad, James P. Wicksted, George S. Dixon, L.P. deRochemont, Journal of Non-Crystalline Solids, 241, (1998) 59-70.

VITA

Robert Ascio

Candidate for the Degree of

Master of Science

Thesis: THE EFFECTS OF INCREASING EUROPIUM AND SODIUM
CONCENTRATION ON THE IONIC CONDUCTIVITY
IN ALUMINOSILICATE GLASSES

Major Field: Physics

Biographical:

Personal Data: Born in Bagio City, Philippines on August 23, 1968, the son of Carmelo Javier Ascio and Amanda Molina-Ascio.

Education: Graduated from Harlingen High School, Harlingen, Texas in May, 1986; received Bachelor of Science degree in Physics from Oklahoma State University, Stillwater, Oklahoma in May, 1998. Completed the requirements for the Master of Science degree with a major in Physics at Oklahoma State University in December, 2000.

Professional Experience: Employed as a research assistant; Oklahoma State University, 1998-2000. Employed as an undergraduate research assistant; Oklahoma State University, 1996-1998, Employed with Creative Labs, Inc., Stillwater, Oklahoma, 1993-1998, Employed with Drummers West Ltd., San Jose, California, 1990-1993, Employed in the United States Air Force, Travis AFB, California, 1986-1990.

